Politecnico di Torino

Master of Science course in MATERIALS ENGINEERING FOR INDUSTRY 4.0

July 2025

Synthesis of Bio-based Conductive Hydrogels

Supervisors

Prof. Massimo Messori

Dr. Camilla Noè

Candidate

Mahtab Bahrami

To my beloved parents, Rita and Ali,
whose love and support have been the foundation of my journey.

To my dear sister and brother-in-law, Mina and Masoud,
whose encouragement and help have always been a source of strength.

And to my lovely niece and nephew, Roshana and Ali,
whose laughter and light remind me of life's true joys.

This work is for you, with all my love and gratitude.

Abstract

This study aimed to synthesize conductive bio-based hydrogels derived from cold-water fish skin gelatin by incorporating silver nanoparticles into a methacrylated gelatin (GelMA) matrix. Phenylbis(2,4,6-trimethylbenzoyl) phosphine oxide-polyethylene glycol modified (BAPO-PEG) was used as the photoinitiator to form a stable hydrogel network in 180 seconds of curing. The electrical resistance of the GelMA/silver hydrogels was measured through an electrical test, which confirmed the influence of relative humidity and silver content. In the dry state, all samples exhibited non-conductive behavior since the silver nanoparticles did not establish a percolating path. As humidity increased, ion mobility in the swollen hydrogel enhanced, and resulted in a six-order-of-magnitude reduction in resistance. After complete hydration, the sample containing the highest silver content demonstrated the best electrical performance, with a resistance of 24.2 Ω, a resistivity of 0.14 Ω.m, and a conductivity of 6.84 $S.m^{-1}$. Moreover, Piezoresistive measurements confirmed that the electrical current increased with compressive strain.

Additionally, mechanical testing indicated that a higher silver content led to an increased elastic modulus, and the swelling degree of crosslinked GelMA improved from 300% in pure water to 624% in silver nitrate solution indicating the enhancement of absorbency. Thermogravimetric analysis (TGA) revealed that silver-free GelMA decomposed at 260 °C in air and 270 °C in argon.

Table of Contents

List of Figures

List of Tables

List of Equations

List of Abbreviations

AgNPs	Silver nanoparticles
AgNWs	silver nanowires
BAPO-PEG modified	Phenylbis(2,4,6-trimethylbenzoyl) phosphine oxide-polyethylene glycol
CNTs	Carbon nanotubes
DLP	Digital light processing
DoM	Degree of methacrylation
DTG	Derivative Thermogravimetry
FTIR	Fourier-transform infrared spectroscopy
GelMA	Gelatin Methacrylyol
GNRs	Gold nanorods
IPN	Interpenetrating network
MAA	Methacrylic Anhydride
PAA	Polyacrylic acid
PAAM	Polyacrylamide
PEDOT: PSS	Poly(3,4-ethylenedioxythiophene): Poly (styrene sulfonate)
PEG	Polyethylene glycol
PEGDA	Polyethylene glycol diacrylate
PHEMA	Poly(2-hydroxyethyl methacrylate)
phI	Photoinitiators
PNIPAM	Poly(N-isopropyl acrylamide)
PVA	Polyvinyl alcohol
RGD	Arginine-glycine-aspartic acid
RH	Relative humidity
SD	Swelling degree
Semi-IPNs	Semi-interpenetrating networks
SLA	Stereolithography
SMU	Source measurement unit
TE	Tissue engineering
TGA	Thermogravimetric analysis

1. Introduction

Hydrogels are polymer networks with a high capacity for swelling due to strong hydrophilic functional groups, such as -NH_2, -COOH, -OH, -$CONH_2$, etc. These networks can be physically or chemically crosslinked to maintain their integrity against dissolution in an aqueous medium [1]. The three-dimensional network of hydrogels has porosity (Fig. 1-1); Hydrogels vary in morphology, average pore size (ξ), and pore size distribution. These factors are influenced by the molar mass of the space between neighboring crosslinks (Mc), and Mc is affected by various preparation techniques [2].

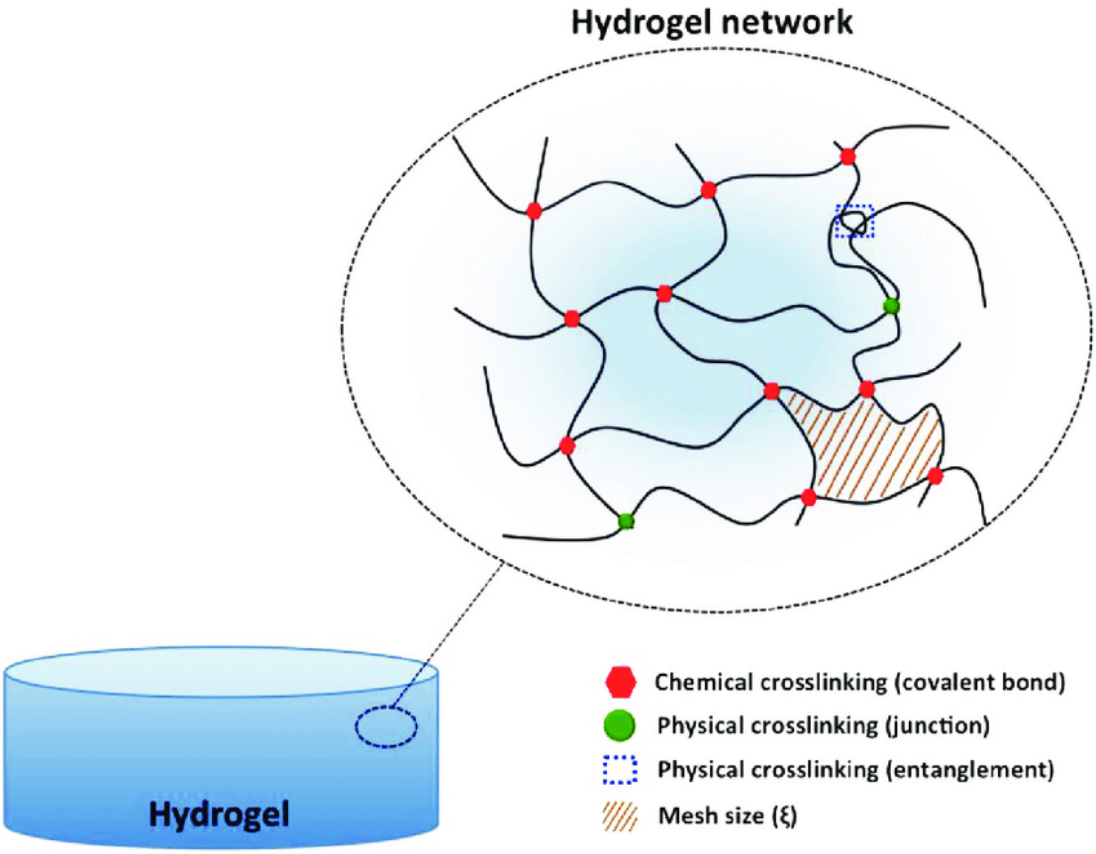

Figure 1-1: Representation of a hydrogel network [2].

Interest in biocompatible hydrogel materials is growing; the objective is to make them appropriate for creating bio-compatible matrices for applications such as drug delivery, wound healing, tissue engineering, and biosensors.

Hydrogels have beneficial physicochemical properties, such as excellent water absorption and permeability. Regarding their formability, they can be formed into thin films and different shapes. By incorporating different natural and synthetic polymers or inorganic nanomaterials,

their functionality and mechanical performance can be enhanced, and advanced hydrogels are created [3].

1.1. Structural and Physicochemical Features of Hydrogels

Hydrogels are classified based on various criteria, as shown in Fig. 1-2.

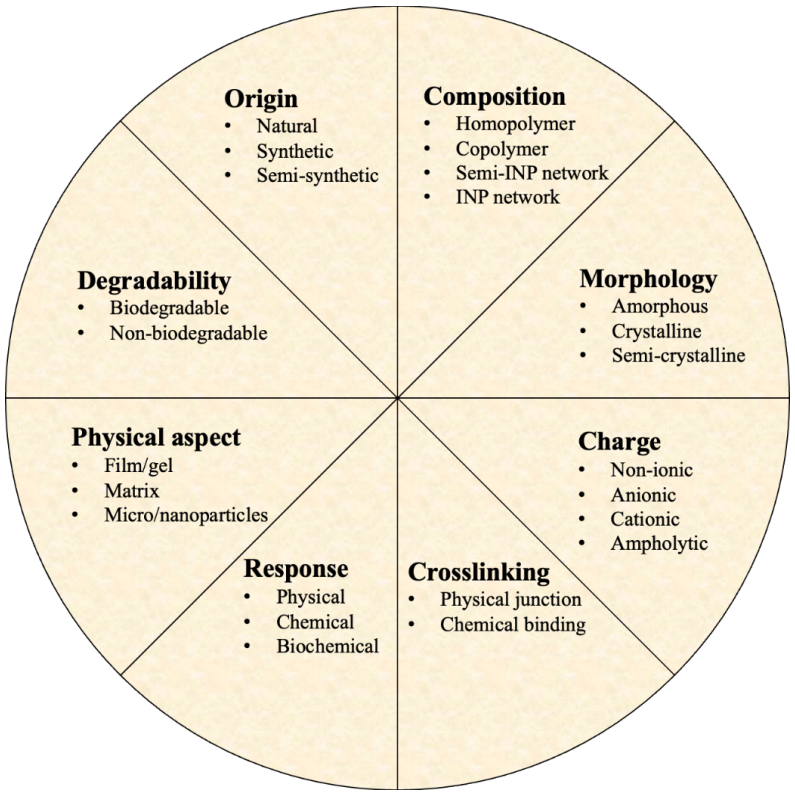

Figure 1-2: Classification of Hydrogels.

Hydrogels are categorized into natural, synthetic, and semi-synthetic types based on the polymer source. Natural polymers, such as polysaccharides (including sodium alginate, chitosan, agarose, hyaluronic acid, and cellulose) and proteins (like collagen, gelatin, elastin, and fibrin), are recognized for their ability to swell in aqueous environments, forming a gel with high water absorption [2][4].

Synthetic polymers containing hydrophilic groups, such as polyvinyl alcohol (PVA), polyethylene glycol (PEG), poly(2-hydroxyethyl methacrylate) (PHEMA), polyacrylic acid (PAA), and polyacrylamide (PAAM), have found large application as efficient water absorbents and have been extensively used to create hydrogels that exhibit excellent mechanical properties. In contrast to natural hydrogels, synthetic ones offer well-defined molecular structures, which are easier to chemically modify and crosslink, resulting in more stable and adjustable networks.

Semi-synthetic or hybrid hydrogels are synthesized by the combination of natural and synthetic polymers or through chemical modifications of natural polymers and provide a balance between bioactivity and mechanical stability [5].

Homopolymer and copolymer hydrogels, semi-interpenetrating networks (semi-IPNs), and interpenetrating polymer network (IPN) hydrogels are classified by polymer chain arrangement, affecting mechanical strength, swelling behavior, and biomedical applications. Homopolymer hydrogels consist of one monomer type, forming networks with repeating structural units. Copolymer hydrogels contain two or more monomer types in varying arrangements, which allows modifications that enhance properties like water absorption, degradation rate, and mechanical stability due to hydrophilic and hydrophobic monomers. Semi-IPN hydrogels have a crosslinked network with uncrosslinked linear chains, that have better swelling and mechanical properties than simple homo- and copolymer hydrogels. IPN hydrogels are formed by the simultaneous gelation of multiple interpenetrated, crosslinked networks and provide excellent mechanical strength, elasticity, and durability. A schematic representation of this classification is shown in (Fig. 1-3) [3][6].

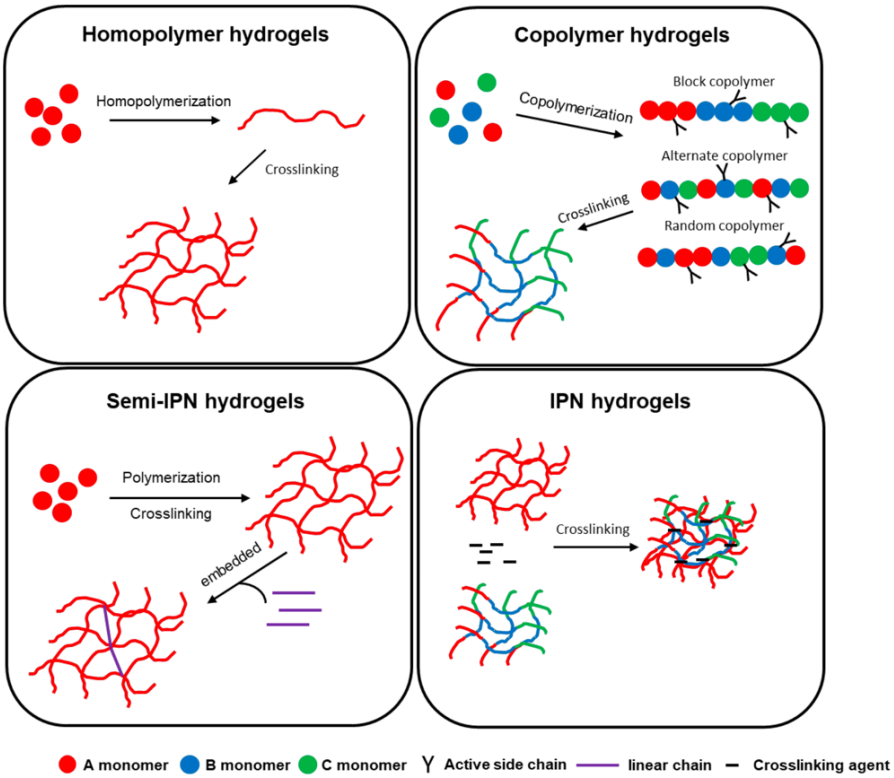

Figure 1-3: Structure of homopolymer, copolymer, semi-INP, and IPN hydrogels [3].

Synthesis of hydrogels is classified into physically or chemically crosslinking methods, using monomers, prepolymers, or polymers. Physically crosslinked hydrogels rely on weak

interactions like hydrogen bonding, self-assembly, crystallization, and ionic interactions without using chemicals [7]. Hydrogen bonding occurs in polymers with N-H, O-H, and F-H groups, enabling reversible hydrogel formation. Self-assembly allows polymers to aggregate in solvents through amphiphilic interactions. Crystallization crosslinking usually requires freeze-thaw or heating-cooling cycles to stabilize networks. Ionic interactions, electrostatic attractions between charged groups, also contribute to hydrogel formation. Crosslinking in protein-modified polymers involves processes like the antibody-antigen effect or functional groups such as hydrogen bonding, improving the hydrogel's structural and bioactive properties [8].

Chemically crosslinked hydrogels are formed via covalent bonding and ensure mechanical stability and durability. It is categorized into chemical reactions, enzymes, high-energy radiation, and free-radical polymerization. Through chemical reactions, complementary functional groups react with a crosslinking agent to create a permanent polymer network. Enzyme-mediated crosslinking uses specific enzymes to catalyze crosslinking in enzyme-sensitive polymers, providing a controlled and biologically compatible hydrogel synthesis approach. High-energy radiation, such as gamma rays or electron beams, generates free radicals that initiate crosslinking. In free-radical polymerization, biocompatible hydrogels are formed through enzyme-catalyzed reactions or UV excitation for biomedical applications [6].

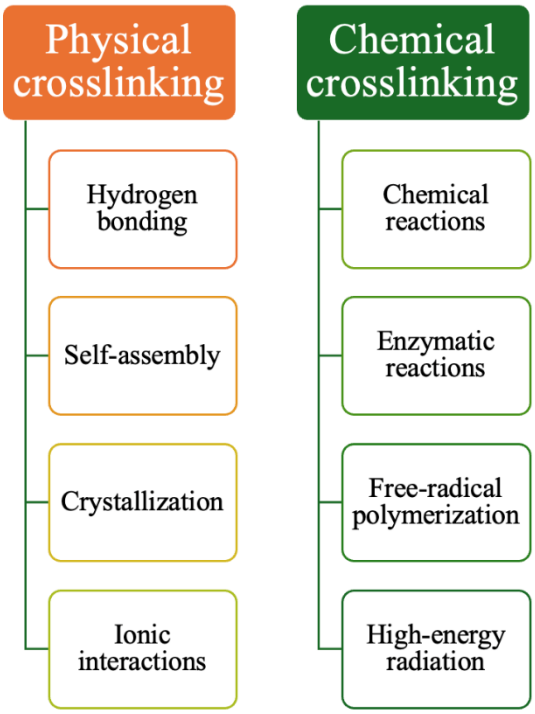

Figure 1-4: Hydrogel synthesis methods.

Recent hydrogel synthesis prioritizes sustainability and biodegradability, leading to innovative methods like the Photon-Fenton method and self-assembly. The Photon-Fenton method creates biodegradable nanogels using sunlight without external crosslinking agents, offering a greener fabrication method. Self-assembly relies on localized chemical interactions for hydrogel formation without chemical crosslinking agents, preserving structural integrity. These techniques improve biocompatibility and promise environmentally friendly hydrogels for biomedical and industrial applications [9].

1.2. Gelatin-based hydrogels

Gelatin is extensively utilized to create hydrogels. It is derived from the partial hydrolysis of collagen, the primary structural protein in animal connective tissues [10]. Its properties ,such as biocompatibility and biodegradability, enable its use in the food industry for gelling, thickening, and stabilizing products such as desserts, pastries, and dairy products, as well as in the pharmaceutical industry for making capsule shells, coatings, and cosmetics [11]. Various animals, such as mammalian and marine species, can be used, which significantly influence the properties of the obtained gelatin. For instance, fish gelatin contains lower proline and hydroxyproline, amino acids that are essential for stabilizing collagen's triple-helix structure. Therefore, lower gelation and melting temperatures, and reduced gel strength are observed in comparison with mammalian gelatin from porcine or bovine [12][13]. Despite these differences, fish gelatin is a sustainable and commercially available raw material that has gained attention as a main byproduct of the fish-processing supply chain [14][15]. Various parts of fish, including the skin, scales, bones, heads, and fins, can be utilized in the production of gelatin [16]. The properties of fish gelatins also differ based on their source; warm-water fish, such as tilapia, and cold-water fish, like cod, have distinct amino acid compositions, which contribute to the differences in their properties [17]. In biomedical applications, gelatin is commonly crosslinked chemically or enzymatically to create biocompatible hydrogels. Regardless of its origin, gelatin polypeptides preserve bioactive sequences, such as arginine-glycine-aspartic acid (RGD), which provide -NH_2, -COOH, and -OH functional groups. Upon cooling, gelatin solutions can form physical gels; however, these gels tend to be weak and show restricted mechanical stability under standard conditions, and they dissolve or degrade slowly [18].

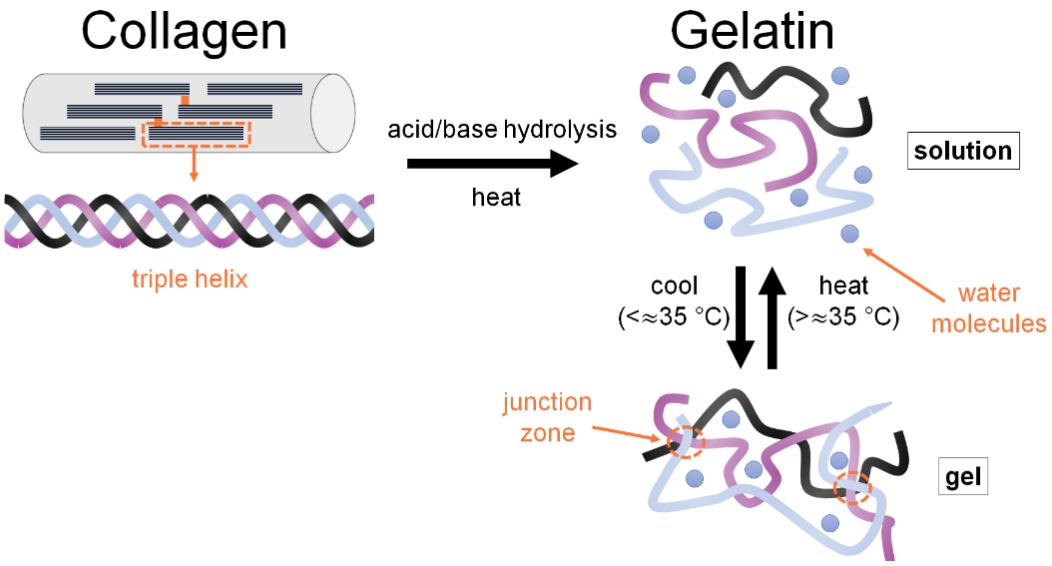

Figure 1-5: Hydrolysis of Collagen.

To enhance the mechanical properties of gelatin or to introduce new functionalities, fish gelatin must be chemically modified. The modification can be accomplished through different techniques: for example, by chemical crosslinking, in a research glutaraldehyde was used as a crosslinking agent and addition of it to a level enhanced the breaking load by a factor of 3.5 times in comparison to uncrosslinked gelatin [19] or by chemical modification such as methacrylation [20], physical treatment using UV irradiation is another technique discussed in the literature, where the gel strength increased after exposing granulated fish gelatin to UV light, which is likely due to the enhanced crosslinking of alkyl and phenyl groups in the side chains as crosslinking sites in the gelatin [21], in another study enzymatic crosslinking using transglutaminase improved gel strength [22]. Similarly, the physical mixing of gelatin-biopolymers was also explored in interpenetrating polymer network (IPN) hydrogels using modified gelatin and sodium alginate to enhance the mechanical properties of both [23].

Methacrylation is a typical approach that involves adding polymerizable groups to generate gelatin derivatives, which can create covalently crosslinked networks [24]. Methacrylate groups contain a C=C bond and are attached to the gelatin backbone, mainly at lysine residues, which, with the cooperation of a photoinitiator, undergo photo-crosslinking upon exposure to visible or UV light [23]. A high methacrylation degree (above 80%) can produce stiffer and more durable hydrogels, while lower degrees produce more flexible variants [20]. GelMA maintains good water solubility, which becomes insoluble after photo-crosslinking, yet it remains able to absorb water and swell. GelMA can be considered a hybrid hydrogel and remains among the most

extensively studied gelatin-based hydrogels due to its straightforward synthesis and ease of use. These hybrid materials benefit from the excellent properties of hydrogels and the induced ability of photo-crosslinking. Changing factors such as formulations, degree of methacrylation (DoM), and light exposure affect their gelation and mechanical properties; therefore, scaffold stiffness for different tissues like cardiac, cartilage, muscle, and bones, which are bioinks in 3D bioprinting, can be tailored [25]. Their ability to be loaded with therapeutic molecules or nanoparticles and gradually release their contents makes them useful in drug delivery [22]. They are widely used in wound healing as bioactive dressings; they maintain a moist environment and deliver growth factors or antimicrobial agents directly to wounds [26]. Regarding tissue adhesives or sealants, natural adhesiveness and modified gelatins are used for effective tissue crosslinking. Gelatin-based hydrogels are versatile and practical in 3D cell culture, organoids, regenerative medicine, and controlled drug release [27].

GelMA itself is electrically insulated, and in order to be used in the field of soft bioelectronics and wearable technology, it must be conductive to transmit electrical signals. There are different strategies to create conductive gelatin hydrogels and bridge the gap between rigid conductive materials and soft, non-conductive ones, making them ideal for applications that need flexibility and electrical properties. These materials have attracted significant interest and are improving day by day [28].

Conductive polymers can be used to create a conductive hydrogel. A research study demonstrated that polypyrrole was grafted onto GelMA through triple crosslinking (thermo-photo-ionically). This resulted in a highly stable and conductive bioink suitable for ink writing-based 3D printing applications [29]. Similarly, the combination of a GelMA precursor with dispersed poly(3,4-ethylenedioxythiophene): poly (styrene sulfonate) PEDOT: PSS, which is a conductive polythiophene, results in the formation of a uniformly conductive hybrid hydrogel [30]. Another example is the successful creation of a high-performance ionically conductive hydrogel made entirely from natural polymers such as gelatin and oxidized sodium carboxymethylcellulose. The hydrogel was immersed in an ammonium sulfate solution, and ionic conductivity was due to the incorporation of mobile ions. This hydrogel displayed outstanding mechanical properties, and was effectively used as a strain sensor, proving its ability to track complex joint movements accurately, and established its significant potential for applications in motion tracking and wearable bioelectronics [31].

Carbon nanotubes (CNTs), carbon nanofibers, and graphene are excellent conductors that can form a percolation path within a hydrogel and create conductive hydrogels. A research study introduced a new microneedle patch embedded with a drug, carbon nanotubes, and GelMA, in

which carbon nanotubes enabled conductivity and provided an interface for cell interaction [32]. Metallic nanoparticles, nanorods, and nanowires possess great conductivity; therefore, they are highly effective in imparting electrical conductivity. In a study, GelMA was integrated with gold nanorods (GNRs) to enhance electrical conductivity and mechanical strength, thereby facilitating the creation of functional cardiac tissue constructs, including cardiac patches. The resultant conductive hybrid hydrogels demonstrated efficacy in supporting cardiac cell adhesion, retention, and spreading, while also promoting uniform expression of cardiac-specific markers and facilitating cell-cell interactions. Furthermore, these hydrogels exhibited robust and synchronized beating at the tissue level [33]. Another study has shown that GelMA with collagen and silver nanowires (AgNW) can create a stimuli-responsive hydrogel actuator that releases the encapsulated molecules upon exposure to an electrical stimulus [34]. Another study showed that direct incorporation of silver nanoparticles into fish gelatin hydrogel during its formation demonstrated extraordinary stretchability, self-adhesiveness, and heightened sensitivity to mechanical stress. These properties enabled it to function effectively as a self-powered wearable strain sensor capable of detecting subtle human movements. Its strain sensitivity enabled real-time monitoring of body motions, making it suitable for applications in soft electronics and biomechanical sensing [35].

Silver is generally considered the most conductive material of all metals and, for this reason, has attracted the most attention among conductive fillers. It can be incorporated into hydrogels such as nanoparticles, nanowires, or microflakes to create a conductive network. This composite is known as conductive hydrogels. Silver nitrate is commonly used to produce silver nanoparticles via chemical or photoreduction. A challenge in creating silver-loaded hydrogels is achieving a homogeneous and uniform distribution to prevent aggregation, thereby maintaining mechanical integrity and electrical conductivity.

To sum up, silver-loaded GelMA hydrogels represent a synthesis of biomaterials and electronic elements, which provides a foundation for the creation of soft, wearable, and functional devices. This union of biological compatibility found in natural polymers like gelatin with remarkable conductivity of silver illustrates the fundamental principle of conductive biobased materials. As research advances, these materials are set to offer significant potential for applications in next-generation health monitoring systems, smart textiles, implantable sensors, and various bioelectronic systems that demand both high-performance conductivity and efficient biocompatibility.

1.3. Absorption Behavior of Hydrogels

The fundamental and desirable property of hydrogels is their ability to swell upon contact with a compatible solvent. When a hydrogel is in its initial state and contacts solvent molecules, molecules of the solvent penetrate the hydrogel. This penetration leads to a significant change in the hydrogel volume. Typically, the water mass fraction in a hydrogel exceeds that of the polymer in its swollen form. Hydrogels have hydrophobic groups oriented outward; however, hydrophilic groups are oriented inward and bound to water molecules via hydrogen bonding. The swelling properties are influenced by numerous factors, including the hydrophilic or hydrophobic nature of the polymeric chains, bonding type, charge, and mainly the extent of porosity and the type of porous structure; hydrogels are classified into four categories: non-porous, micro-porous, macro-porous, and super-porous hydrogels based on the porous structure. For instance, hydrogels that are crosslinked using hydrophilic polymers exhibit more significant swelling than those crosslinked with hydrophobic polymers [36]. Factors such as time, temperature, pH, and the surrounding medium have a significant influence on swelling behavior. It is evident that the longer the hydrogels are in contact with the solvent, the greater the extent of swelling until they reach equilibrium [37].

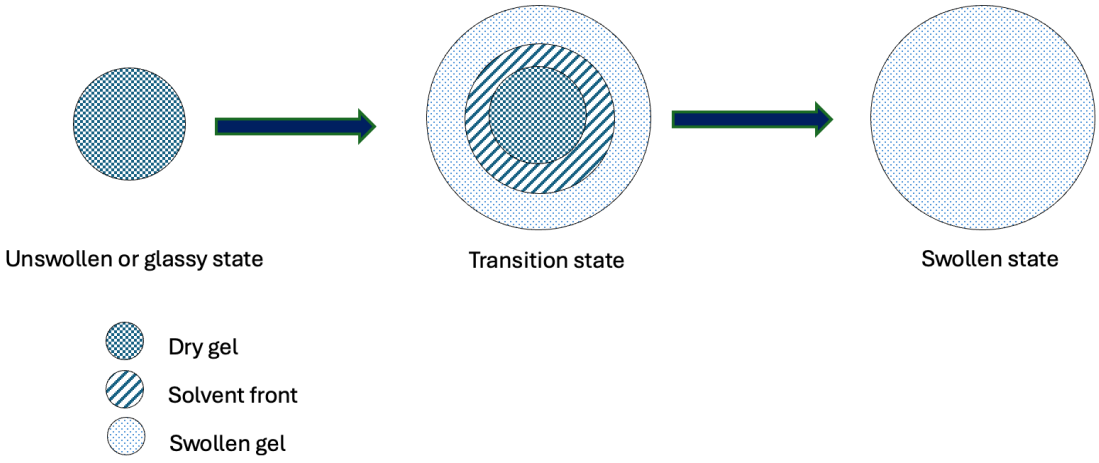

Figure 1-6: Swelling behavior of a hydrogel.

Determining the swelling properties is essential for establishing the stability of a hydrogel. The swelling degree is obtained based on the equilibrium, which is calculated by Equation 1-1.

Equation 1-1

$$SD(\%) = \frac{W_t - W_d}{W_d} \times 100$$

The total solvent uptake can be calculated using Equation 1-2, which shows the quantity of solvents absorbed by the hydrogel.

Equation 1-2

$$Solvent\ content(\%) = \frac{W_t - W_d}{W_t} \times 100$$

Where W_t is the weight at time t, W_d is the weight of the dry sample.

1.4. Photocurable Hydrogel Systems

Photocurable hydrogels are photosensitive systems that include photoinitiators (phI), polymers or prepolymers (e.g., GelMA), fillers, and additives. Under the exposure of the light (UV [200-400 nm] or visible [400-800 nm]), photoinitiators absorb photons and produce reactive species, such as free radicals, which initiate the crosslinking, and a hydrogel network is created under mild conditions [38]. Photoinitiators are classified into two groups of Type I and Type II; Type I breaks into radicals after light absorption, and Type II needs a co-initiator to produce radicals [39]. Photocuring proceeds through chain-growth by generating free radicals that react with polymer vinyl groups (e.g., methacrylate) and form C–C crosslinks. Photocurable hydrogel formulation offers the opportunity to get integrated into advanced fabrication techniques, such as 3D printing through digital light processing (DLP) or stereolithography (SLA) [40].

Phenylbis(2,4,6-trimethylbenzoyl)phosphine oxide-PEG(BAPO-PEG) is a type I photoinitiator and is water soluble; it generates radical species under the exposure of UV or visible light. It contains a BAPO core, known for its ability to efficiently generate radicals, and its solubility in water is enhanced by polyethylene glycol modifications [41]. This reagent is a pale-yellow powder and shows strong absorbance in the UV and visible spectrum, and has high initiation efficiency, which makes it suitable to start light crosslinking in a wide range of photocurable systems such as GelMA hydrogels.

1.5. Conductive Hydrogels Systems

Conductive hydrogels have gained increasing attention in biomedical applications because they have tissue-like mechanical properties, they are soft, stretchable, and, in some cases, self-healing. Their ability to create conformable and biocompatible interfaces offers distinct advantages over traditional rigid electronic components, particularly in the context of wearable and implantable devices. They are also recognized as excellent materials for flexible electronics and biomedicine. Their durability against mechanical deformations, like stretching and bending, makes them suitable for wearable and implantable devices. With customized designs, these hydrogels convert mechanical stimuli into measurable electrical signals through changes in resistance or capacitance. Unlike conventional rubber-like substrates coated with conductive nanomaterials, which often lack biocompatibility and risk skin irritation or material detachment, conductive hydrogels ensure compatibility with biological tissues. They are ideal for applications in strain sensors, supercapacitors, touch panels, triboelectric nanogenerators, and various bioelectronic interfaces that demand effective signal conversion and skin interaction conformity [42].

One of the challenges in developing conductive hydrogels is achieving stable integration of additives within the polymer network to prevent phase separation, which compromises mechanical and electrical performance. Thus, strong interactions between the polymer matrix and conductive components are essential for long-term stability and functionality.

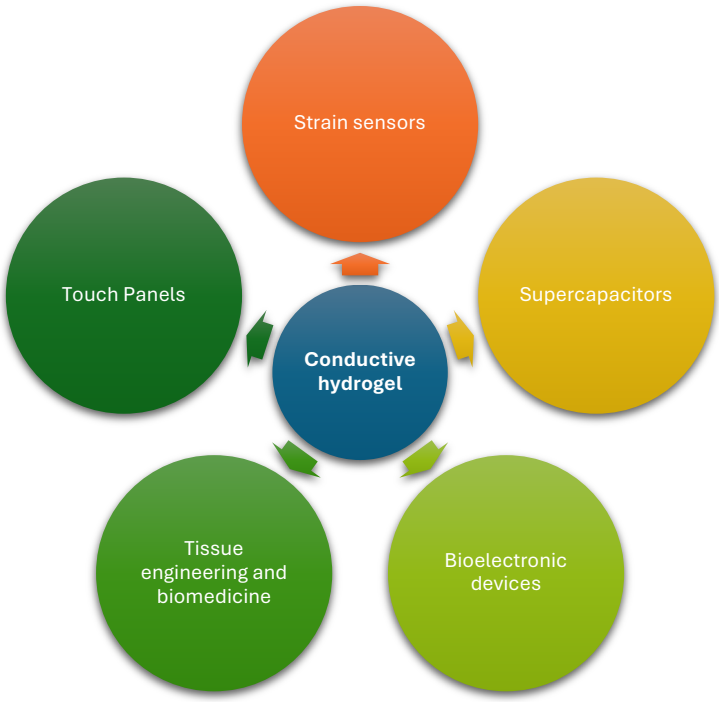

Figure 1-7: Conductive hydrogels applications

1.6. Aim of study

Gelatin methacryloyl (GelMA) hydrogels are widely studied in biomedical applications, such as tissue engineering and drug delivery. Their capabilities in wearable electronics and biosensors are attracting increasing attention. Even with advancements, there always remain opportunities to improve GelMA's functionality, particularly by incorporating conductive features and enhancing its environmental responsiveness. Modifying these materials is useful for developing sustainable and adaptable electronic platforms, since it decreases dependence on synthetic materials.

Gelatin derived from the cold-water fish skin is a renewable, commercially available alternative to mammalian gelatin. It has characteristics such as biocompatibility and biodegradability. Methacrylated gelatin (GelMA) exhibits photo-crosslinking properties, which enable the formation of stable hydrogel networks under mild conditions.

A challenge in creating conductive hydrogels is incorporating conductive materials, such as silver nanoparticles. The influence of direct silver nitrate addition on gelation kinetics and network characteristics requires examination. Additionally, Phenylbis(2,4,6-trimethylbenzoyl)phosphine oxide-PEG (BAPO-PEG), a water-soluble type I photoinitiator, shows potential for rapid gelation. Exploring the influence of silver content and humidity on the electrical performance of wearable biosensors is essential for their effective use.

This research aims to fulfill several primary objectives:

- Synthesis of a bio-based conductive hydrogel using GelMA, which is obtained from gelatin derived from cold-water fish skin.
- Exploring the optimal amount of BAPO-PEG required for photo-crosslinking, to optimize both gelation speed and polymer network formation.
- Investigate how the in situ generation of silver nanoparticles impacts the gelation kinetics and develop a solution to effectively incorporate silver nanoparticles.
- Assess the electrical performance of the synthesized hydrogel across various salt formulations and humidity levels.

2. Materials and Experimental Methods

2.1. Materials

Gelatin from cold-water fish skin, methacrylic anhydride, $AgNO_3$, sodium hydroxide, calcium chloride, and sodium chloride were supplied by Sigma-Aldrich and used as received. BAPO-PEG was synthesized starting from regular Phenylbis(2,4,6-trimethylbenzoyl)phosphine (BAPO) and was kindly provided by Dr. Andrea Cosola for this study. All materials were used without further pre-treatment.

2.2. Synthesis of Methacrylated Gelatin

Gelatin (15 g, 15 wt%) was dissolved in distilled water in a flask, and the mixture was stirred at 50 °C until the gelatin was completely solubilized, yielding a clear solution.

Once the gelatin was fully dissolved, methacrylic anhydride (MAA) (0.58 mL of methacrylic anhydride per gram of gelatin) was added dropwise to the solution under continuous stirring over 10 minutes. The solution pH was kept constant at eight by adding NaOH solution (1 M) when needed after checking it with pH paper. The reaction proceeded for 4 hours at 50 °C under constant stirring until it was complete. During this time, methacrylic anhydride molecules reacted with the free amine groups (mainly lysine residues) on gelatin, attaching methacrylate functional groups. This process yields GelMA macromers, where gelatin contains vinyl groups capable of photo-crosslinking [43].

GelMA was dialyzed in deionized water for 7 days to remove the methacrylic acid, remaining methacrylic anhydride, and other impurities. After dialysis, the GelMA solution was freeze-dried, obtaining a fluffy white compound (Fig. 2-3).

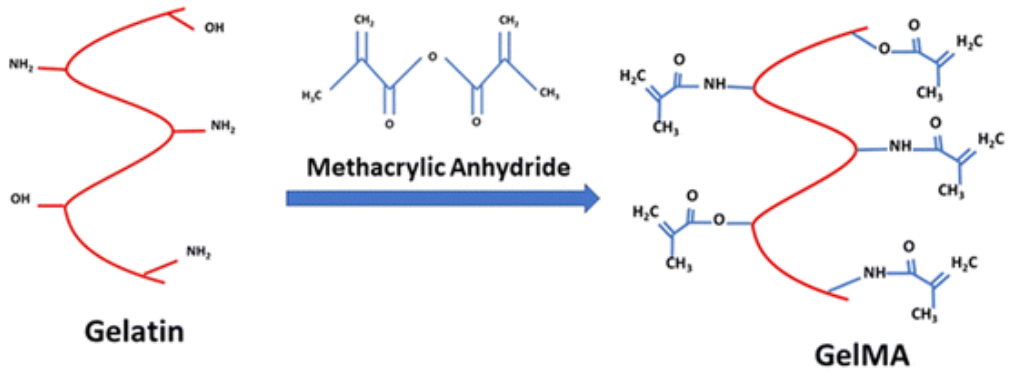

Figure 2-1: The schematic of GelMA synthesis [44].

Table 2-1: Summary of reaction parameters.

Parameter	Value
Gelatin concentration	15 wt%
Reaction temperature	50 °C
MAA: Gelatin ratio	0.6 g : 1 g
pH during reaction	8
NaOH concentration	1 M
Reaction time	4 hours
Dialysis duration	7 days
Freezing temperature	–20°C, –80°C

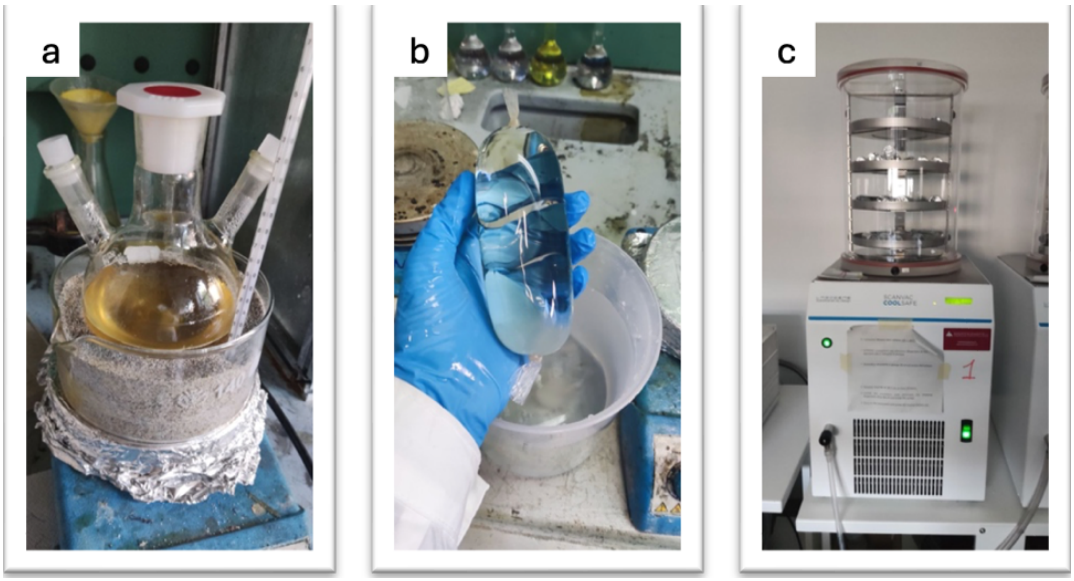

Figure 2-2: a) Synthesis set-up, b) Dialysis, c) Freeze-Dryer.


Figure 2-3: Freeze-dried GelMA.

2.3. Photo-crosslinking of GelMA

Freeze-dried GelMA (2 g, 20 wt%) was dissolved in an aqueous solution with the photoinitiator (BAPO-PEG), and it was stirred for 5 minutes until a homogeneous solution was achieved. BAPO-PEG was added at 0.5, 1.5, 3, and 4 phr (per hundred resin) relative to the GelMA (for example, for 0.5 phr of phI, 10 mg of BAPO-PEG was used per 2 grams of GelMA). The mixture was stirred until the photoinitiator was fully dissolved, producing a clear, pale yellow polymer solution.

The polymer solution was pipetted onto the quartz plate of the photorheometer and underwent crosslinking upon exposure to a broad-range visible light fiber optic lamp. The mixture quickly became more solid as exposure continued, indicating the formation of a hydrogel network. Under light exposure, BAPO-PEG breaks down to generate radical species that react with the methacrylate double bonds in GelMA, leading to chain polymerization and crosslinking of the gelatin chains into a covalent network.

Figure 2-4: The schematic of photo-crosslinking[44].

Table 2-2: Formulations of GelMA and BAPO-PEG.

GelMA Concentration	BAPO-PEG (phr)
20 wt%	0.5
	1.5
	3.0
	4.0

2.4. Incorporation of Silver Nitrate

Silver nanoparticles were incorporated into GelMA hydrogels using two methods: (1) direct mixing (before crosslinking) and (2) immersion (after crosslinking). Both aimed to load silver

nanoparticles into the hydrogel, enabling conductivity. All silver sample handling occurred in low light to prevent premature photoreduction.

2.4.1. In Situ Loading

In the direct mixing method, silver nitrate was mixed with the GelMA polymer solution before crosslinking. The precise amounts of $AgNO_3$ (15, 20, and 30 phr of $AgNO_3$ relative to the GelMA amount were dissolved easily in the polymer solution (20 wt% GelMA in distilled water with 4 phr phI), resulting in a clear solution. The solution was then pipetted onto the quartz glass of the photorheometer. During the curing process of the silver-loaded polymer solution, a brown color was observed, indicating that Ag^+ ions were being reduced to elemental silver (Ag^0), and a clear, mirror-like surface was evident on the surface of the crosslinked GelMA, which additionally indicated the formation of metallic silver (Fig. 2-5). Literature supports this observation, showing that photoinitiator systems can reduce metal ions under UV and visible light. Thus, the direct mixing method generates a GelMA/silver hydrogel in a single step, where silver is simultaneously introduced and partially converted to nanoparticles as the network forms. However, this method is effective for a thin layer of hydrogel; in thicker samples, light penetration is limited, therefore, real-time silver reduction is not feasible.

Equation 2-1: Dissociation of silver nitrate in aqueous media.

$$AgNO_3(s) \rightarrow Ag^+(aq) + NO_3^-(aq)$$

Equation 2-2: Reduction of silver ion.

$$Ag^+(aq) + e^- \rightarrow Ag^0(s)$$

Table 2-3: Different formulations with silver nitrate.

Prepolymer solution	Silver nitrate (phr)
GelMA + 4 phr phI	15
	20
	30

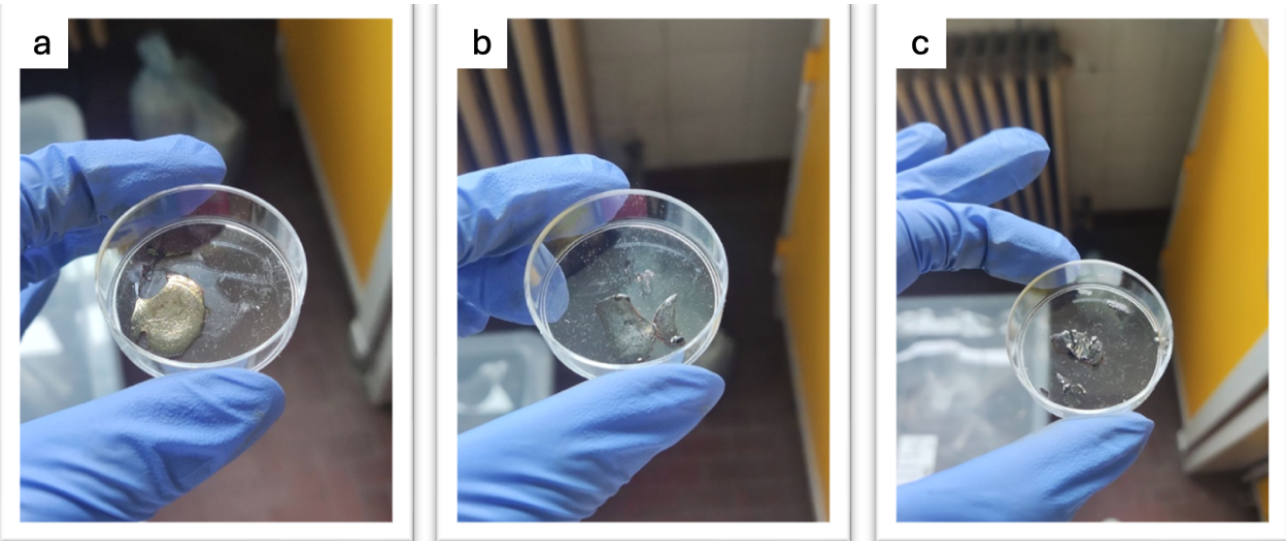

Figure 2-5: Crosslinked GelMA containing 4 phr of BAPO-PEG and varying concentration of silver nitrate; a)15 phr, b)20 phr, and c)30 phr.

2.4.2. Immersion

GelMA hydrogels free of silver were prepared for the immersion method (Fig. 2-6). They were immersed in three solutions of $AgNO_3$ with varying concentrations in deionized water to enable the Ag^+ ions to diffuse into the network. This method is preferable since it no longer influences photo-crosslinking and is effective for both thin and thick samples. Each sample was put into a separate container filled with silver nitrate solution, which was subsequently wrapped in aluminum foil to shield the hydrogels from light during the swelling test.

After performing the swelling test, the hydrogels were kept in the silver nitrate solutions for 19 days without coverage, to allow sufficient time for Ag^+ to diffuse into the gel matrix. The choice of an extended 19-day soaking period aimed to ensure an even distribution. To enhance the uniformity of silver ion distribution, the samples underwent a short period of sonication during the immersion process. As immersion continued, they achieved better uniformity.

In GelMA, functional groups such as $-NH_2$, -OH, and -COOH can reduce silver ions upon long exposure to light, in addition to the contribution of phI to the reduction. The formation of silver nanoparticles observed during the 19-day immersion in ambient light is due to a slow sunlight-driven reduction process similar to that found in natural organic matter. Research indicates that sunlight can reduce silver ions in materials with chemical groups, without any photoinitiator [45]. Over time, an obvious color change occurred; the hydrogels resulted in a dark brown color by the end of the immersion period, which indicates silver reduction and the formation of metallic nanoparticles throughout the network (Fig. 2-7). The hydrogels were removed from the silver nitrate solution, and excess liquid was gently removed. They were then freeze-dried and

resulted in brown and brittle GelMA/silver hydrogels (Fig. 2-8). This dehydration process solidified the hydrogel, preventing silver leaching during handling. The color of the freeze-dried samples was lighter compared to prior dehydration, and they did not appear to be perfectly uniform. The sample obtained from immersion in a 50 wt% silver nitrate solution was covered with a visible white surface layer, which can be the precipitation of silver salt ($AgNO_3$ or a derivative).

This method mimics processes that produce sustained-release antimicrobial hydrogels, where a polymer scaffold absorbs a drug or ion through soaking [46]. For my experiment, soaking the crosslinked GelMA in $AgNO_3$ provided a straightforward method to incorporate silver nanoparticles into the hydrogel.

Both methods, pre-mixing and immersion, produced GelMA/silver hydrogels.

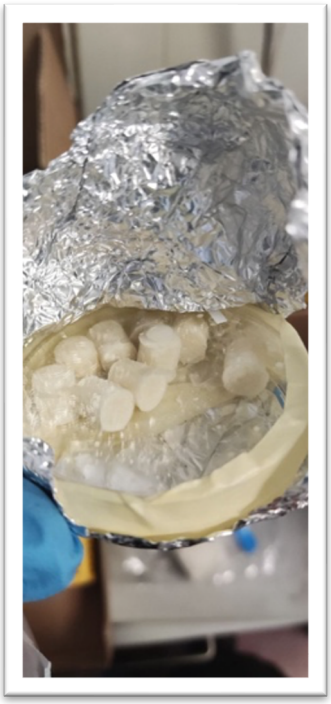

Figure 2-6: Crosslinked GelMA without silver.

Table 2-4: Different formulations of silver nitrate solution.

Crosslinked sample formulation	Silver nitrate solution (wt%)
20 wt% of GelMA + 3 phr phI	30
	40
	50

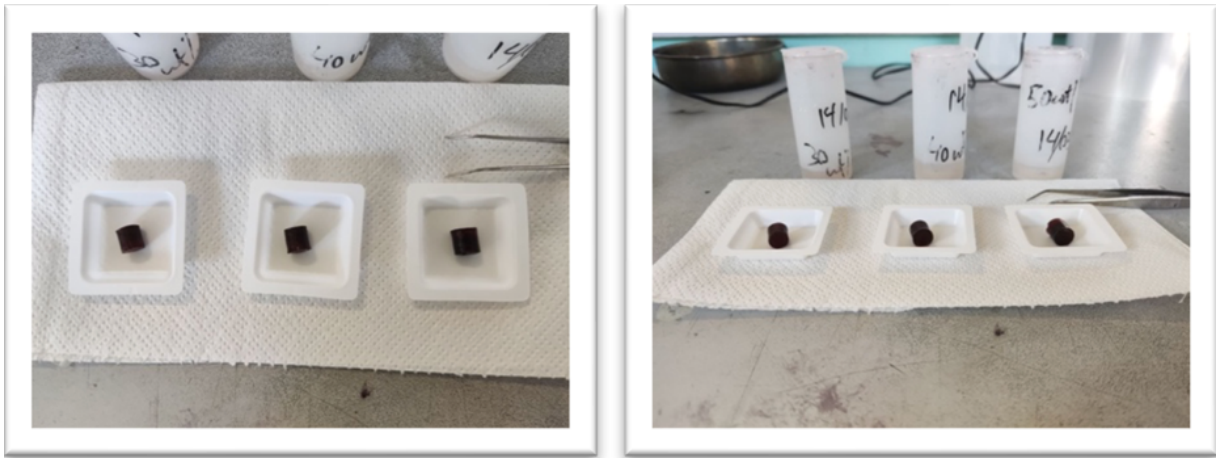

Figure 2-7: GelMA/silver hydrogel before freeze-drying.

Figure 2-8: Freeze-dried GelMA/silver hydrogel.

2.5. Relative humidity environment

To evaluate the influence of humidity on the electrical performance of GelMA/silver hydrogels, samples were maintained in three distinct controlled humidity environments before conducting the electrical test. Specific relative humidity levels were established using saturated salt solutions of calcium chloride ($CaCl_2$) for 32% relative humidity (RH) and sodium chloride (NaCl) for 72% RH. For complete hydration, they were immersed in distilled water. Samples were placed in sealed chambers containing the corresponding solutions and allowed to equilibrate at room temperature for 7-12 days, or until a constant weight was achieved, to ensure uniform moisture absorption and distribution (Fig. 2-9).

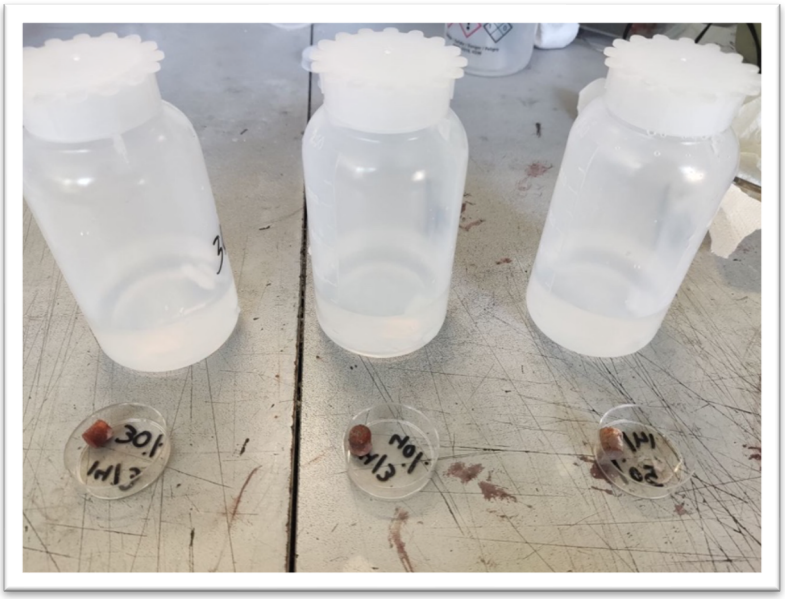

Figure 2-9: Sealed chambers for a humid environment.

2.5.1. Fourier Transform Infrared Spectroscopy (FT-IR)

Fourier Transform Infrared (FTIR) spectroscopy is a non-destructive analytical method used to identify chemical bonds and functional groups in materials by examining their absorption of infrared light. Chemical bonds exhibit different vibrational frequencies, leading to the absorption of IR light at specific wavenumbers, which are characteristic of bond strength and atom masses. The spectrometer uses a Michelson interferometer to modulate the infrared (IR) beam and create an interferogram, which gives a time-domain signal that is further transformed into a frequency-domain spectrum using a Fourier Transform operation.

The unique absorption bands in the resulting spectrum can be compared to established reference data to determine functional groups. Typically, an Infrared Spectroscopy Absorption Table is utilized to link the observed peaks with their corresponding bond types and vibrational modes (such as C=O stretching and N–H bending). These tables help the analysis of FTIR spectra, especially in the context of complex or altered polymer systems.

Fig. 2-10 illustrates the Thermo Fisher Scientific Nicolet iS50 FT-IR spectrometer used for spectral acquisition. The instrument features an ATR (attenuated total reflectance) accessory that directly measures solid or gel-like samples with little preparation. Spectral analysis was done, utilizing OMNIC software (Thermo Fisher Scientific), which enables the processing of absorbance spectra and supports comparison with reference databases.

Figure 2-10: Nicolet iS50 FT-IR spectrometer

2.5.2. Photorheological Characterization

The curing kinetics of GelMA were characterized by photorheology using a visible-light source. In a typical photorheological setup, the sample is placed between a two-plates configuration and oscillatory shear stress or strain is applied to measure its mechanical response while it gets irradiated by a light source. The setup allows to record changes in storage modulus (G′), loss modulus (G″), and viscosity during the curing process.

During the time-sweep experiment, initially the material behaves like a low-viscosity liquid; when irradiated, crosslinking reactions are triggered, leading to an increase in the storage modulus (G′), which reflects the material's elastic properties. The point at which G′ exceeds G″ indicates the gel point, which signifies a transition from liquid-like to solid-like behavior.

The photorheology test was conducted using a parallel plate configuration with a diameter of 25 mm and a quartz bottom plate to allow light transmission, with a 300 µm gap between them. A constant strain amplitude (γ of 1%) was applied at a frequency of 1 Hz, and the lamp was turned on after a 30-second stabilization period, and the light intensity used was 28 mW/cm².

2.5.3. Thermogravimetric Analysis

Thermogravimetric Analysis (TGA) is a thermal analysis method that monitors the mass of a sample as the temperature gradually increases. The primary goal of TGA is to assess a material's thermal stability and composition by tracking weight changes during heating. In a typical TGA experiment, a small sample, typically in a dry state, is placed on a microbalance within a furnace. The temperature is then increased at a controlled rate (for example, 10°C per minute) in either

an inert atmosphere (such as argon or nitrogen) or air. This test provides information such as the onset decomposition temperature, which indicates the start of significant weight loss, and the thermal stability limit. The temperature at which the maximum decomposition rate occurs is often identified by analyzing the first derivative of the TGA curve (DTG), which appears as a peak and helps compare stability or analyze multi-step degradation, as well as the residue fraction at elevated temperatures. In hydrogel research, these parameters offer insights into the material's thermal resistance and composition.

Figure 2-11 shows a Setaram TGA system that features a Mettler Toledo TGA/DSC gas control module, which accurately regulates the type and flow of gases entering the chamber. This setup facilitates controlled transitions between inert and oxidative environments, which are crucial for examining different phases of thermal degradation.

Figure 2-11: Setaram TGA system with a Mettler Toledo TGA/DSC gas control

2.5.4. Swelling test

Swelling tests are widely used to assess materials' liquid absorption capacity and impact on weight, volume, or dimensions. This phenomenon occurs when a porous or polymeric material absorbs a solvent, usually water or a buffer, resulting in physical expansion. Molecular structure, crosslink density, and the interaction between the material and the solvent significantly influence this property.

The sample is dried in a standard swelling experiment to determine its initial mass. Subsequently, it is immersed in an excess of swelling medium for specific time intervals and until it achieves equilibrium. Once removed, the sample is lightly wiped to remove the surface liquid, and then its swollen weight is measured.

Swelling is commonly expressed as a swelling degree (SD), $SD\% = \frac{W_t - W_d}{W_d} \times 100$ where W_t is the weight at time t and W_d is the initial, dry weight.

By tracking this ratio over time, researchers can assess the balance of swelling capacity and its rate. Swelling experiments can be conducted on a range of materials, including hydrogels, elastomers, smart polymers, membranes, and polymer composites. These assessments offer valuable information about solvent absorption patterns, internal network configurations, and reactions to changes in the environment.

2.5.5. Electrical Test

A vertical mechanical testing apparatus equipped with a force sensor from Nordic Transducer (NTT, Denmark) is designed to apply controlled compressive or tensile forces to material samples. This setup features a movable upper crosshead and a stationary lower platform that securely holds the specimen in place. Copper contact plates can be incorporated into the fixture to serve as both mechanical clamps and electrical interfaces, enabling simultaneous electromechanical measurements. Electrical connections to these plates are usually made using standard cables or alligator clips. The system can be connected to a source measurement unit (SMU), such as the SMU4201 by Aim-TTi, to assess electrical properties. The SMU provides precise sourcing and measurement capabilities, allowing for applying a fixed voltage while simultaneously measuring current. This setup permits real-time resistance monitoring. LabView software from National Instruments controls and synchronizes the system's mechanical and electrical components, enabling automated testing sequences, real-time data gathering, and coordination between load application and electrical measurements.

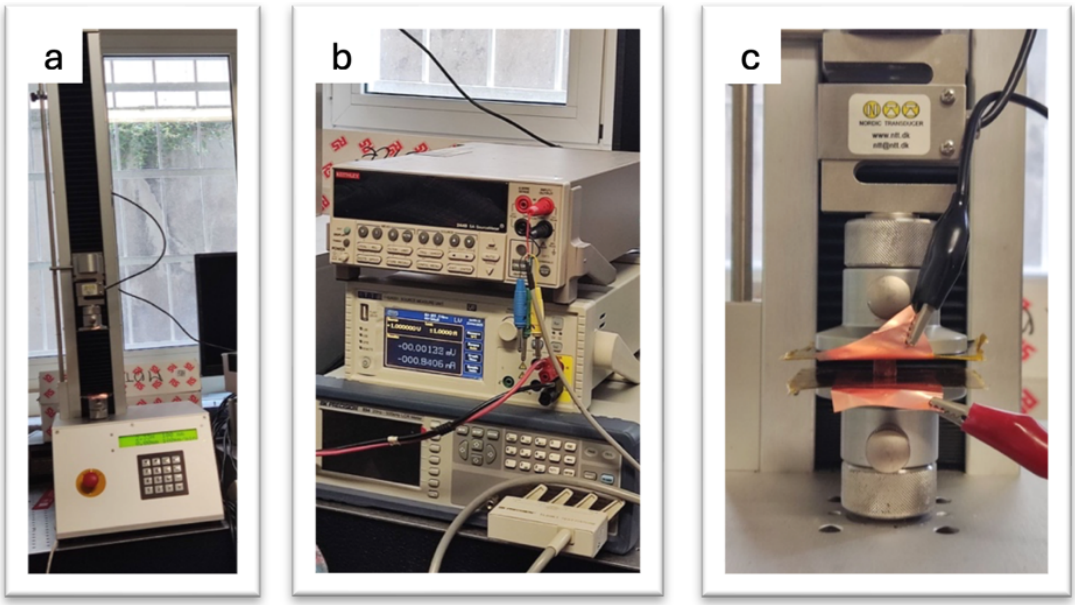

Figure 2-12: a) Vertical mechanical testing system, b) Source measurement unit 4201 by Aim-TTi, c) close-up of sample mounted between sopper electrodes.

Piezoresistive and compression tests were carried out using the same mechanical testing equipment equipped with a displacement actuator. The parameters, speed, displacement, and preload are set by the THSSD-2024 software (GripSoft, Germany). During each test time, the way (displacement) and load values are recorded for each sample. Each test was performed with a preload of 0.05 N, a displacement of 2 mm, and a constant speed of 5 mm/min in 20 seconds.

3. Results and discussion

3.1. Characterization by FTIR

FTIR spectra were obtained for unmodified gelatin and GelMA, using the same instruments and settings, spanning the range of 550–4000 cm^{-1}, with a resolution of 4 cm^{-1}, at room temperature. All samples were examined in solid form using the ATR accessory, which enabled direct surface measurements.

3.1.1. Gelatin from cold-water fish skin

The FTIR spectrum of fish gelatin displayed clear bands that are characteristic of its protein structure. A broad absorption band around 3300 cm^{-1} was detected, which is associated with Amide A, resulting from N–H stretching vibrations in peptide bonds and O–H stretching in hydroxyl groups. The Amide I band, located near 1650 cm^{-1}, corresponds to the C=O stretching of the peptide backbone and is typically the most significant absorption feature in protein FTIR spectra. The Amide II band, seen around 1540 cm^{-1}, arises from a combination of N–H bending and C–N stretching, indicating that the peptide bonds remain intact. Additionally, the Amide III band, found at approximately 1240 cm^{-1}, results from C–N stretching and N–H deformation, further confirming the protein composition [47][48].
These results confirm the structural integrity of the unmodified gelatin.

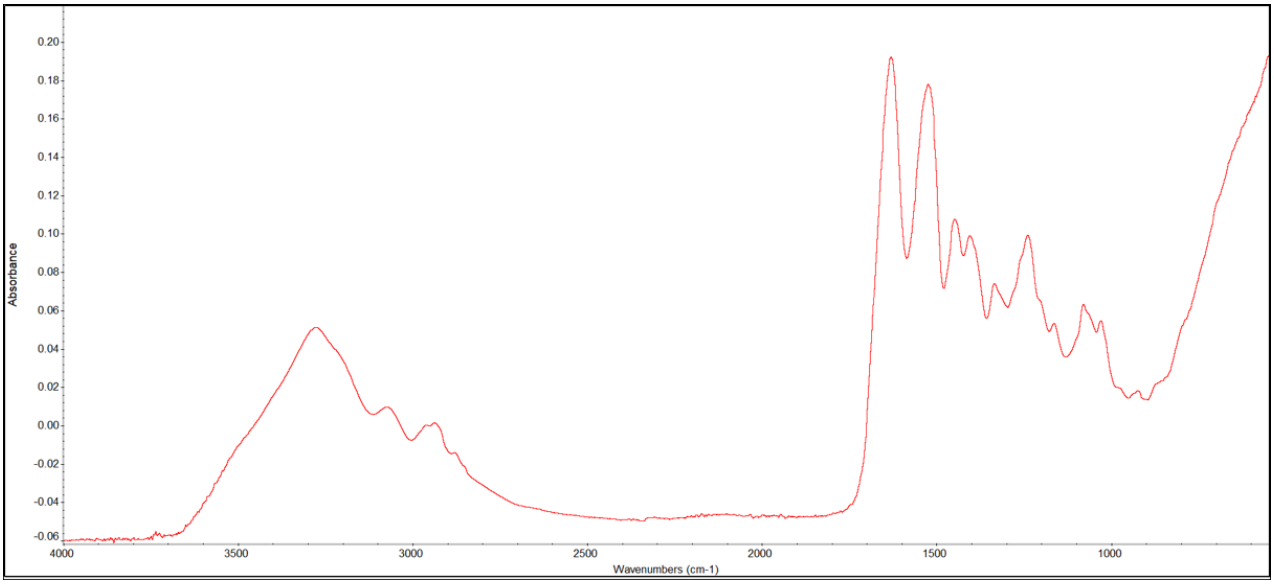

Figure 3-1: FTIR spectrum of Gelatin before methacrylation reaction.

Table 3-1: Characteristic bonds of Gelatin.

Wavenumber (cm^{-1})	Bonds
3300	Amide A: N–H stretching and O–H stretching
1650	Amide I: C=O stretching of peptide bonds
1540	Amide II: N–H bending and C–N stretching
1240	Amide III: C–N stretching and N–H deformation

3.1.2. Methacrylated gelatin

Fig. 3-2 shows FTIR spectra of unmodified gelatin and synthesized GelMA. Although a distinct C=C stretching band near 1635 cm^{-1} was not observed, likely due to overlap with the Amide I band. The reduction in band intensity around 3300 cm^{-1} (Amide A), 1650 cm^{-1} (Amide I), and 1540 cm^{-1} (Amide II) indicates partial consumption of N–H and O–H functional groups during the methacrylate reaction, especially those linked to lysine and hydroxy-containing amino acids. The FTIR spectrum does not confirm the methacrylation, but the modification is supported by its performance, in which, after the addition of photoinitiator, it underwent photo-crosslinking. This phenomenon happens when photosensitive methacrylate groups are available.

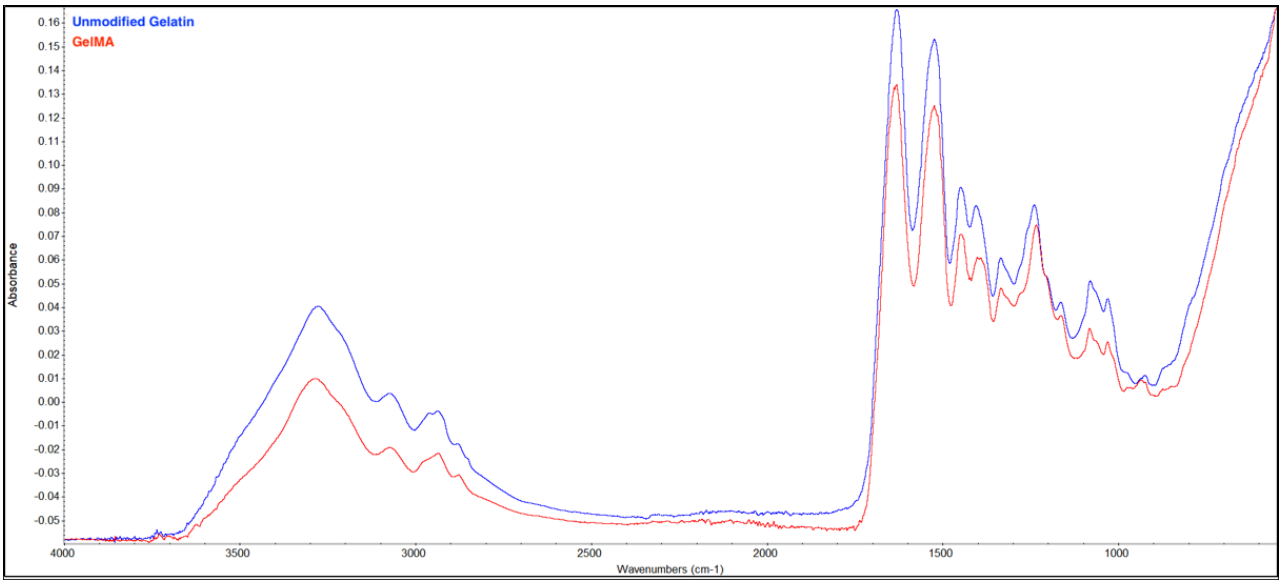

Figure 3-2: Comparison of FTIR spectra of Gelatin before and after methacrylation.

3.2. Evaluation of gelation behavior by photorheology

Photorheology tests were carried out within the linear viscoelastic region (LVR), and all experiments were performed at room temperature and repeated three times to ensure accuracy.

3.2.1. Methacrylated gelatin

The photoreactivity of the methacrylated gelatin was evaluated using real-time photorheology. At first, the storage modulus (G′) is low, indicating that the GelMA solution is liquid-like and uncrosslinked. As the photoinitiation process begins (onset time), crosslinking starts, causing a sharp increase in G′, which signifies a shift to a more elastic and solid-like state. Eventually, the modulus reaches a plateau once the crosslinking reaction is finished, resulting in no further solidification. Higher concentrations of BAPO-PEG led to quicker crosslinking (shorter induction times) and greater final G′ values (Fig. 3-3). This finding supports the notion that higher initiator concentrations accelerate the photopolymerization process.

This trend indicates that higher concentrations of photoinitiators led to a greater generation of radicals, which speeds up crosslinking and shortens gelation time. Table 3-2 shows that increasing the BAPO-PEG concentration from 0.5 to 3 phr reduces the onset time and gelation time from 80 to 56 s and from 85 to 59 s, respectively. The induction time, defined as the difference between the gelation time and the onset time, shows the speed of the gelation process once it has started, which also decreased from 5 to 3 s by increasing the photoinitiator, which suggests a highly efficient crosslinking process. The rate of gelation indicated by $\Delta G'/\Delta t$ increased from 3.71 to 9.33 $Pa.s^{-1}$, demonstrating faster curing. However, increasing the concentration of photoinitiator from 3 to 4 phr did not change the onset time, gelation time, and induction time, and $\Delta G'/\Delta t$ demonstrated only a slight increase. This indicates that increasing the amount beyond 3 phr does not enhance crosslinking under the given light conditions. Therefore, 3 phr is considered the ideal concentration for gelation, as it helps prevent potential issues such as unnecessary expenses related to excess photoinitiator. The lamp was turned on after 30 seconds, with the storage modulus stabilizing at approximately 210 seconds. Therefore, a 180-second exposure to visible light was sufficient for full curing of the material. Research shows that the amount of photoinitiator mainly influences the gelation kinetics rather than the ultimate stiffness, given sufficient light exposure.

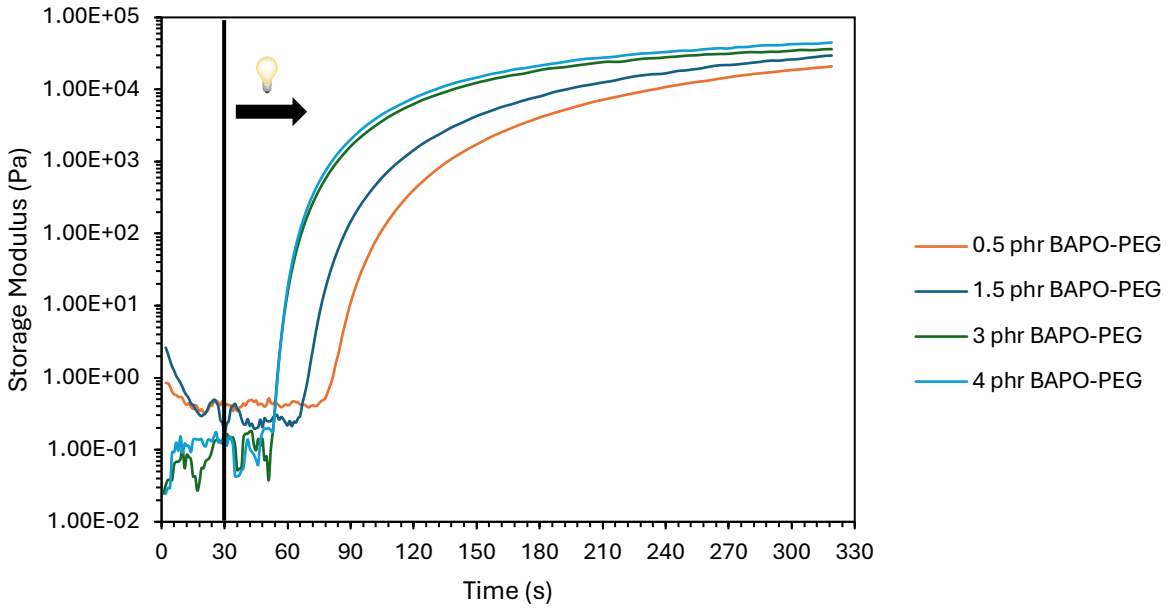

Figure 3-3: Comparison of photorheology curve recorded for 20 wt% GelMA solubilized in water with different concentrations of BAPO-PEG.

3.2.2. Methacrylated gelatin with silver nitrate

Silver nitrate was added to GelMA solutions with 4 phr photoinitiator because earlier findings indicated that no considerable difference between 3 and 4 phr was observed regarding gelation time and final modulus. Since 3 phr seemed to be the optimal concentration, no further addition of photoinitiator was done, and the experiment moved forward with 4 phr to avoid preparing a new solution with 3 phr to prevent using more material.

At a fixed concentration of photoinitiator of 4 phr, the amount of silver nitrate ($AgNO_3$) was increased from 15 to 30 phr, resulting in a progressive increase in the induction time from 4 seconds to 22 seconds, along with a decrease in the gelation rate from 4.91 to 2.43 $Pa.s^{-1}$. The onset times showed slight variation, ranging from 56 to 62 s, compared to the silver-free GelMA solution, but there was a significant increase in gelation time and therefore induction time, indicating that the presence of Ag^+ ions substantially delays gelation after the initiation phase. As the concentration of silver nitrate increases, the plateau storage modulus (G′) gradually decreases. These findings indicate that the presence of silver ions (Ag^+) interferes with the photo-crosslinking process by preventing the penetration of light . While low concentrations of silver (e.g., ≤10 phr) have minimal effects, the higher concentrations applied in this study (15-30 phr) significantly hinder network formation and overall mechanical strength [49].

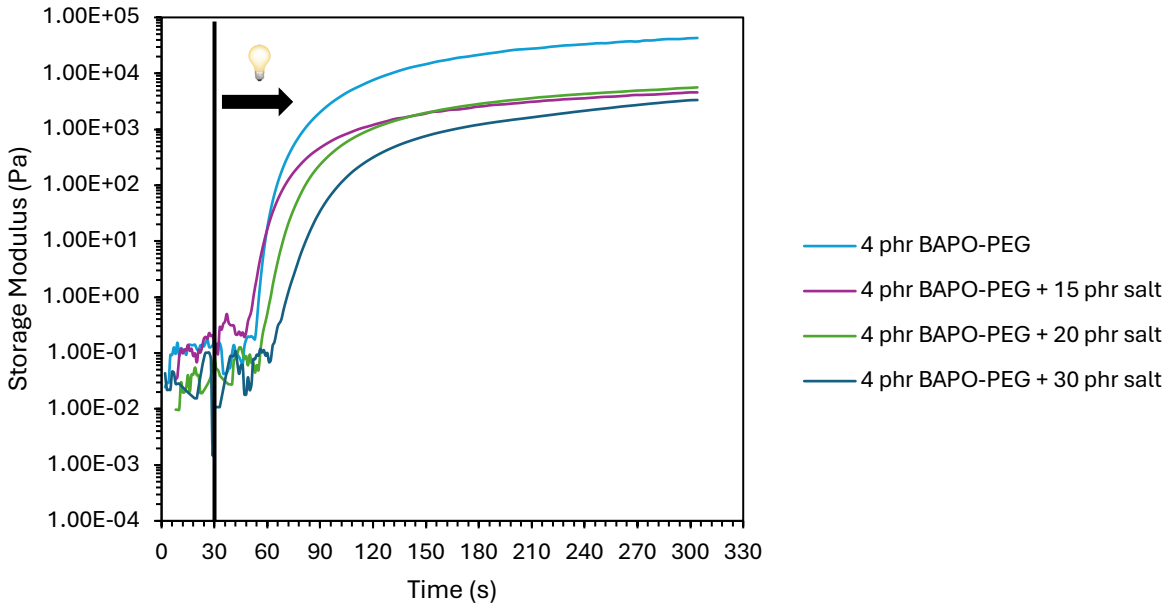

Figure 3-4: Comparison of photorheology curve recorded for 20 wt% GelMA solubilized in water with 4 phr BAPO-PEG and different concentrations of $AgNO_3$.

Table 3-2: Induction times and Storage Modulus for GelMA hydrogels with different concentrations of BAPO-PEG photoinitiator and silver nitrate.

Formulation	Photoinitiator (phr)	Silver Nitrate (phr)	Onset Time (s)	Gelation Time (s) G′ = G″	Induction Time (s)	ΔG′/Δt ($Pa.s^{-1}$)
GelMA + BAPO-PEG	0.5	0	~80	~85	5	3.71
GelMA + BAPO-PEG	1.5	0	~68	~73	5	5.27
GelMA + BAPO-PEG	3	0	~56	~59	3	9.33
GelMA + BAPO-PEG	4	0	~56	~58	2	11.4
GelMA + BAPO-PEG + $AgNO_3$	4	15	~51	~56	4	4.91
GelMA + BAPO-PEG + $AgNO_3$	4	20	~54	~69	15	3.89
GelMA + BAPO-PEG + $AgNO_3$	4	30	~62	~84	22	2.43

3.3. Thermogravimetric analysis

The test was conducted in triplicate to ensure accuracy under both air and argon atmospheres, at temperatures ranging from 25 to 800 °C with a heating rate of 10 °C/min.

Fig. 3-5 shows the distinct thermal degradation profile of crosslinked GelMA with 3 phr BAPO-PEG in an air atmosphere, as determined by Thermogravimetric analysis and Derivative Thermogravimetry (DTG). A slight mass loss was observed between 30 and 200 °C, accompanied by a minor DTG peak at approximately 190 °C, which can be attributed to the

evaporation of absorbed moisture, a characteristic behavior of hydrogels. The onset temperature (T_{onset}) was identified at 260 °C, signifying the start of considerable decomposition. A significant weight loss occurred between 200 and 450 °C, with a sharp DTG peak located at around 350 °C, corresponding to the thermal decomposition of the GelMA matrix and photoinitiator. Between 450 and 700 °C, oxidative degradation of more thermally stable residues was observed. Above 700 °C, the residual components exhibited stability, resulting in a final char residue of 5.36% at 800 °C.

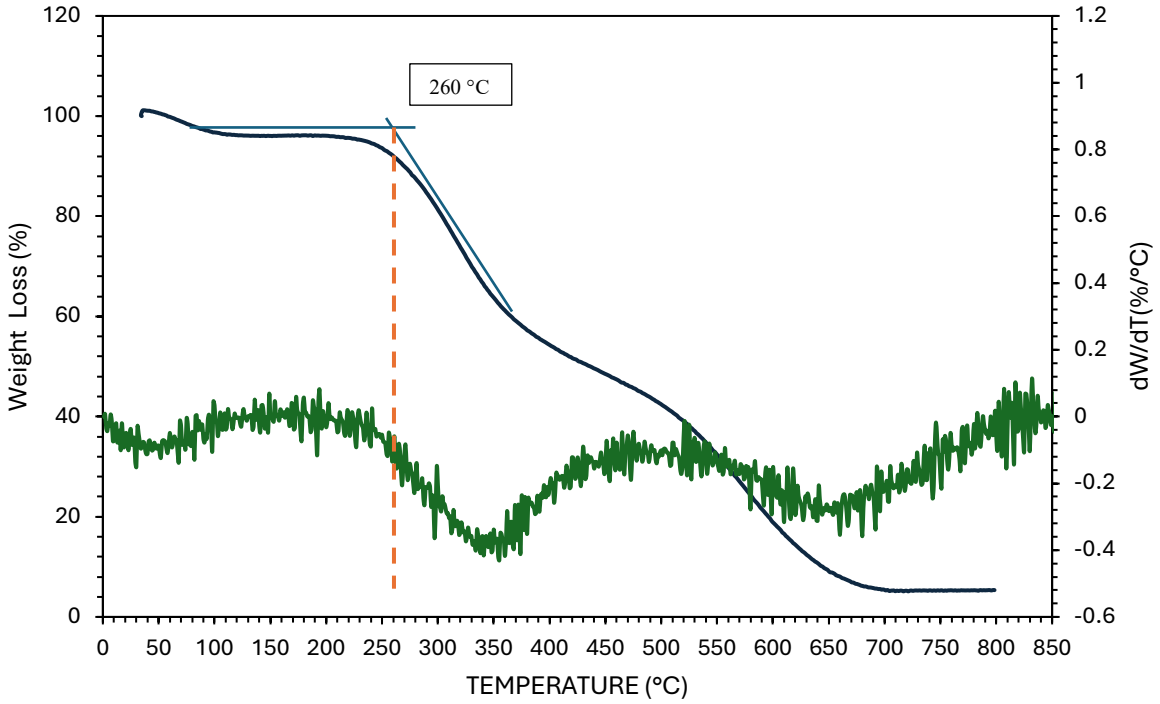

Figure 3-5: Thermogravimetric analysis and DTG of crosslinked GelMA in air.

TGA and DTG curves of GelMA with 3 phr BAPO-PEG, conducted in an argon environment (Fig. 3-6), reveal a three-stage thermal decomposition process [50]. The initial two stages resemble those observed in air, with a minor weight loss occurring between 30 and 200 °C due to the evaporation of absorbed moisture. The onset temperature (T_{onset}) was determined to be 270 °C. The most significant weight loss occurs between 200 and 500 °C, characterized by a distinct DTG peak at around 360 °C, indicating the thermal breakdown of the GelMA network, along with the residual photoinitiator. In contrast to the sample examined in air, there is no DTG peak observed above 500 °C, which confirms the absence of oxidative degradation. After 500 °C, the rate of weight loss stabilizes, resulting in a final char residue of 29.41% at 800 °C [15].

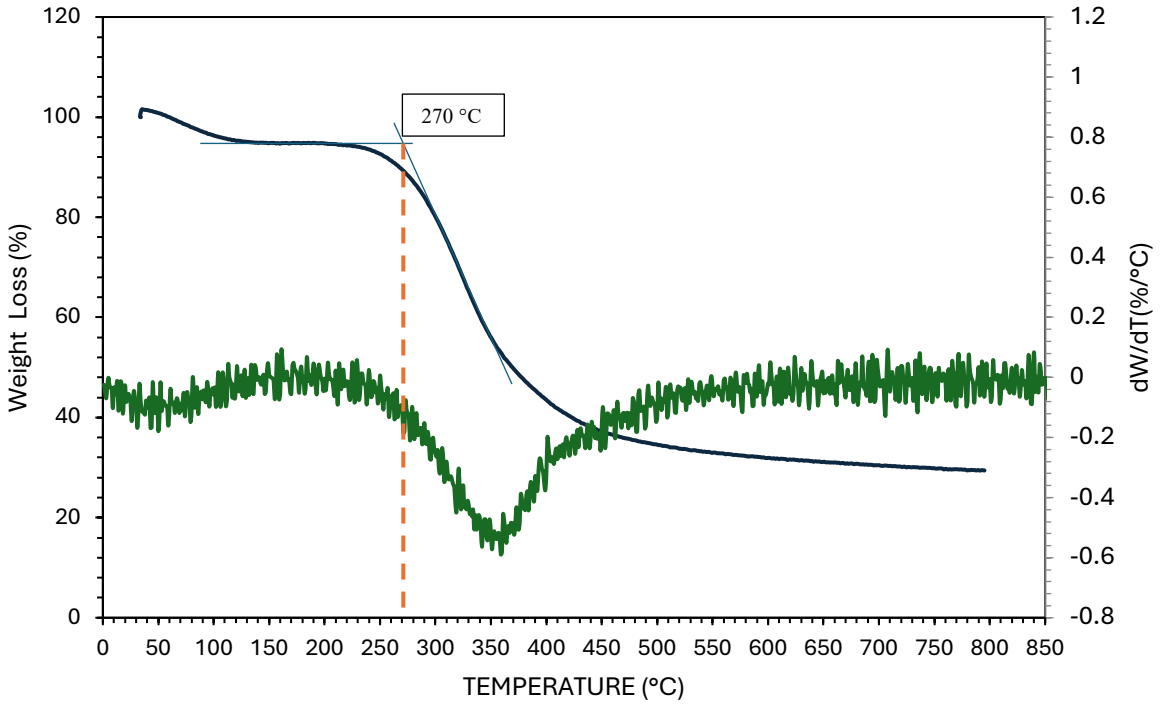

Figure 3-6: Thermogravimetric analysis and DTG of crosslinked GelMA in Argon.

In the presence of air, crosslinked GelMA undergoes oxidative degradation, and cause earlier mass loss. This process is succeeded by the oxidative breakdown of more thermally stable residues containing lower char residues. This difference highlights the critical role of the testing environment in influencing the thermal properties of GelMA.

Table 3-3: Thermal behavior of GelMA in different testing environments.

Testing environment	T_{onset} (°C)	Initial Weight (mg)	Weight at 800 °C (mg)	Char residue (%)	degradation steps	Temperature of peaks (°C)
Air	260	7.02478	0.37611	5.36	Water evaporation	~190
					Decomposition of the GelMA matrix and photoinitiator	~350
					Oxidative degradation of more thermally stable residues	~650
Argon	270	6.187	1.8197	29.41	Water evaporation	~190
					Decomposition of the GelMA matrix and photoinitiator	~360

3.4. Swelling behavior

Crosslinked GelMA samples were immersed in distilled water or in a silver nitrate solution at room temperature, and weight gain measurements were recorded at time intervals of 1, 2, 3, 4, 5, 10, 20, 30, 40, 50, 60, 90, and 120 minutes.

3.4.1. In water

As mentioned before, hydrogels have hydrophilic functional groups and a porous structure, which enables them to absorb a large amount of water; therefore, they show significant swelling behavior. The sample demonstrated a notable increase in swelling within the first 5 to 10 minutes, indicative of rapid water absorption. After 50 minutes, the rate of swelling slowed, ultimately reaching a stabilization point of approximately 300% after 300 minutes (Fig.3-7). This plateau indicates a state of equilibrium swelling and indicates that there is no osmotic pressure difference between inside the hydrogel and its environment, at which the hydrogel does not absorb any further water. The initial rapid absorption of water, subsequently followed by a plateau, exemplifies the two-phase behavior characteristic of these hydrogels.

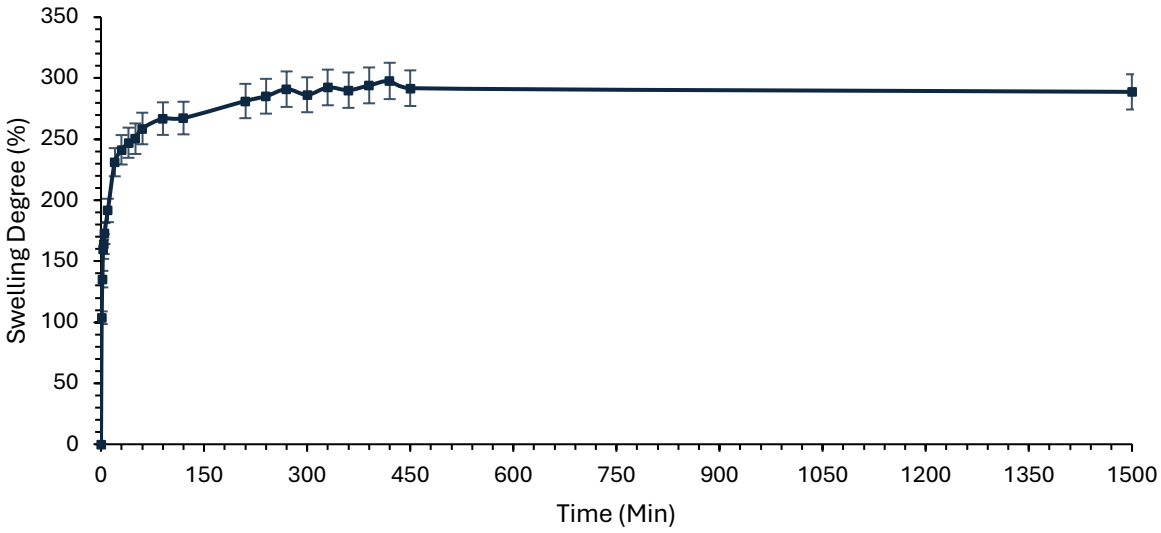

Figure 3-7: Swelling curve of crosslinked GelMA in water.

The sample exhibits a significant increase in water content during the initial minutes. After 50 minutes, the water content is approximately 75% and gradually stabilizes at 300 minutes. This stability suggests an equilibrium in water retention (Fig. 3-8).

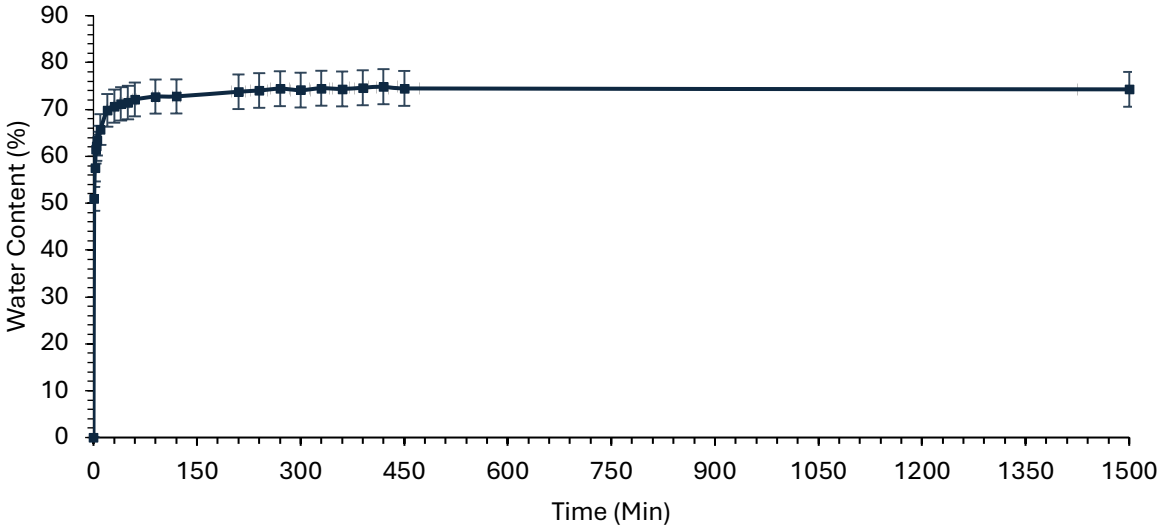

Figure 3-8: Water content curve of crosslinked GelMA.

There is a correlation between swelling and water content, whereby an increased degree of swelling indicates a higher water content.

$SD(\%) = \frac{W_t - W_d}{W_d} \times 100 = 300\%$ $\quad\quad$ $W_t = 4W_d$

$WC(\%) = \frac{W_t - W_d}{W_t} \times 100$ $\quad\quad$ $WC\% = \frac{4W_d - W_d}{4W_d} \times 100 = \frac{3}{4} w_d \times 100 = 75\%$

At equilibrium, the sample exhibited a swelling degree of approximately 300%. By applying this value to Equation 1-1 to determine the ratio between the initial weight and the weight at equilibrium, and substituting the ratio into Equation 1-2, the water content of 75% was calculated, which supports the observed data and confirms the correlation between swelling and water content.

3.4.2. In silver nitrate solutions

The degree of swelling of hydrogels over time was evaluated at various concentrations of $AgNO_3$: 30 wt% (solution A), 40 wt% (solution B), and 50 wt% (solution C). The sample immersed in solution C exhibited the highest degree of swelling, reaching approximately 624% at equilibrium. The samples in solution A and solution B showed swelling degrees of approximately 450% and 512%, respectively. Silver nitrate solutions are acidic, with pH values from about 5 in solution A to 4 in solution C. This supports literature findings that gelatin-based hydrogels swell more as pH decreases below the isoelectric point (pH≈6). Therefore, greater swelling at higher $AgNO_3$ concentrations can be attributed to the acidic environment, which

promotes more ionization of functional groups in gelatin and enhances water absorption. This is similar to an observation in a paper where the swelling capacity increased by moving away from the isoelectric point [51].

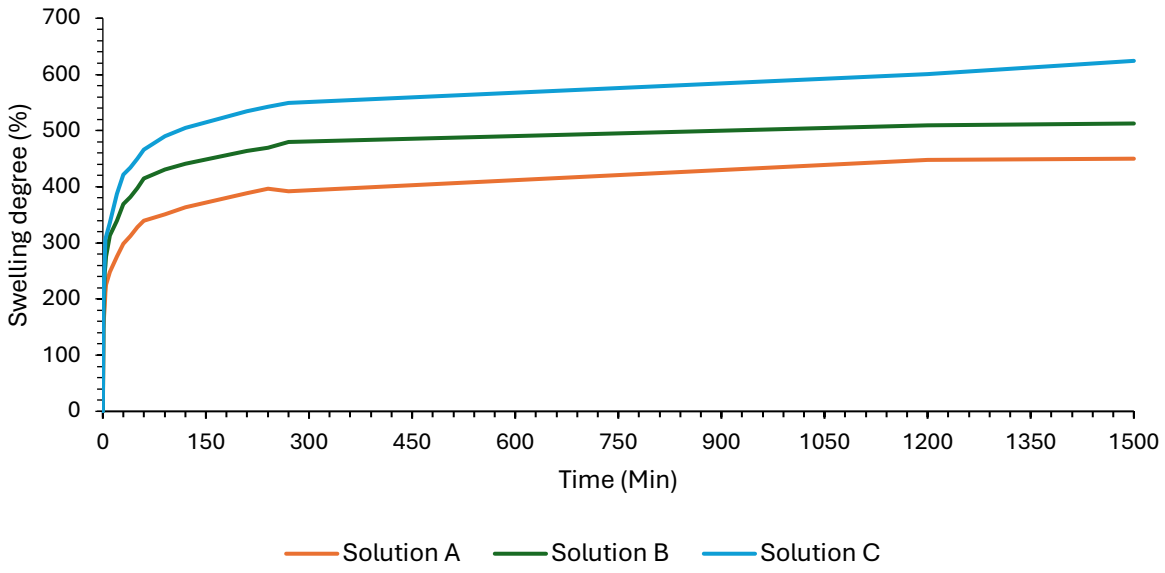

Figure 3-9: Swelling curve of crosslinked GelMA in varying concentrations of silver nitrate solution.

The sample in solution C showed the highest uptake at around 86.1%, followed by solution B and solution A. This consistency supports the conclusion that higher concentrations of $AgNO_3$ enhance absorption under these conditions.

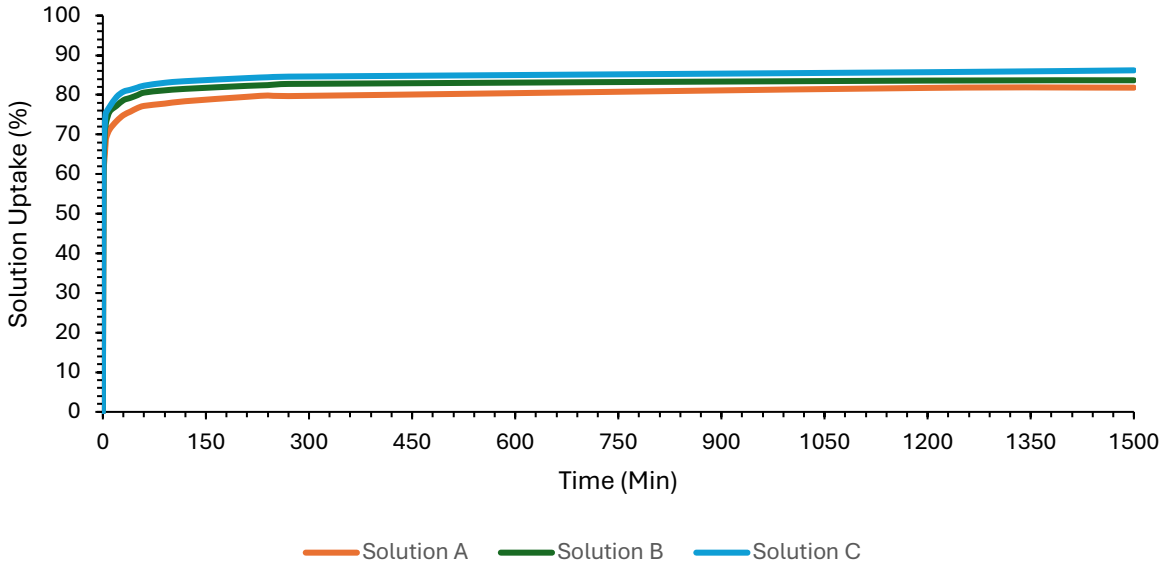

Figure 3-10: Solution uptake curve of crosslinked GelMA in varying concentrations of silver nitrate solution.

The swelling degree of GelMA increased in silver nitrate ($AgNO_3$) solutions compared to pure distilled water (Fig. 3-11).

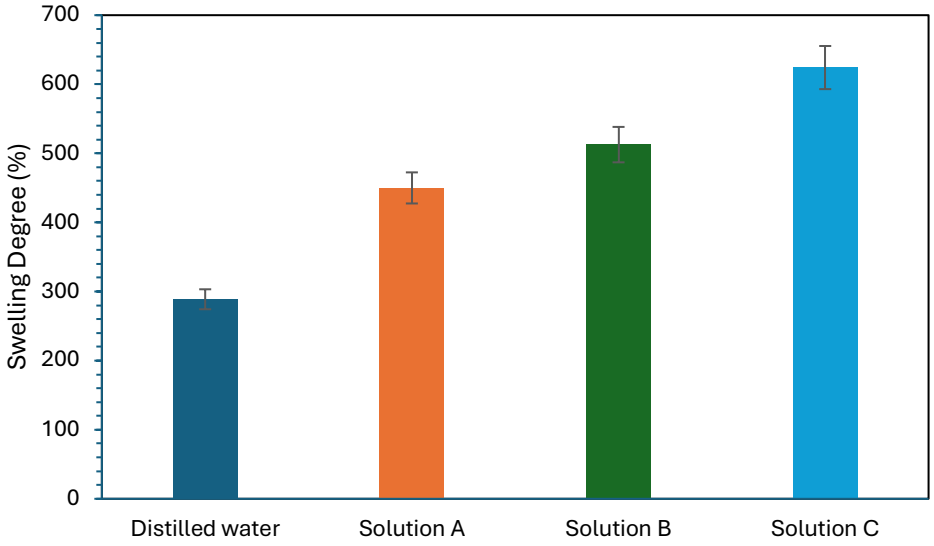

Figure 3-11: Swelling degree of crosslinked GelMA in different media.

3.5. Evaluation of the electrical properties

Measurements of electrical conductivity were performed on GelMA/silver hydrogel samples using a two-probe setup at different humidities. Each cylindrical hydrogel sample was placed between electrodes linked to a source meter, and current–voltage (I–V) characteristics were collected in ambient conditions. The slope of the I–V curves is used to determine the electrical resistance; resistance is inversely proportional to the slope. First, all samples underwent freeze-drying for measurement in the dry state. The quantity of silver in each sample was determined by subtracting the mass of freeze-dried silver-loaded samples from the mass of samples before the swelling test. The amounts of silver inside were measured as 0.2447, 0.3173, and 0.5368 g, corresponding to silver nitrate solutions with concentrations of 30 wt% (GelMA/Ag-30), 40 wt% (GelMA/Ag-40), and 50 wt% (GelMA/Ag-50), respectively.

All hydrogels, after immersion in $AgNO_3$ solution, exhibited a dark color, which confirms the synthesis of silver nanoparticles (AgNPs) within the gelatin matrix (Fig. 2-8). Electrical measurements of dried GelMA/Ag hydrogels conducted under an applied voltage within the ±20 V range revealed extremely high resistance (200-1000 MΩ) and showed that the samples are not conductive in the dried state due to the lack of a connection between silver nanoparticles. While research has indicated that increasing the silver content reduces resistance, which is attributed to the formation of a conductive percolative path. [52]. The weird trend of increasing resistance by increasing silver content in the dry state can be attributed to the measurement unit system

limitation and the fact that these samples are not conductive, so a conclusion of a trend is unreasonable.

Table 3-4: Electrical Characteristics of dried GelMA/silver hydrogels.

Sample	Quantity of silver inside (g)	Slope(A/V)	Resistance (MΩ)
GelMA/Ag-30	0.2447	5×10^{-9}	200
GelMA/Ag-40	0.3173	2×10^{-9}	500
GelMA/Ag-50	0.5368	1×10^{-9}	1000

Gelatin has hygroscopic behavior, and absorbing moisture affects its electrical properties. This swelling enhances the spacing between polymer chains, enhances ion mobility, and increases ionic conductivity. Research findings suggest that an increase in relative humidity (RH) leads to a notable reduction in the resistance of gelatin-based sensors [53][54].

The conductivity of each sample with 32% relative humidity (RH) was measured using the same setup in the range of ±42 V. The samples continued to exhibit high resistance and remained insulators.

Table 3-5: Electrical Characteristics of GelMA/silver hydrogels with 32% RH.

Sample	Quantity of silver inside (g)	Slope(A/V)	Resistance (MΩ)
GelMA/Ag-30	0.2447	3×10^{-9}	333
GelMA/Ag-40	0.3173	2×10^{-9}	500
GelMA/Ag-50	0.5368	2×10^{-9}	500

By further increasing the relative humidity (RH) to 72% and in the range of ± 20 V, the electrical behavior of samples enhanced significantly; the sample exhibited approximately five orders of magnitude less resistance compared to 32% RH, and resistance values decreased from mega-ohm (MΩ) to kilo-ohm (kΩ). The I-V curves were linear and ohmic; however, the GelMA/Ag-50 could not complete the experiment, as it burned, likely due to excessive applied voltage (Fig. 3-12(b)).

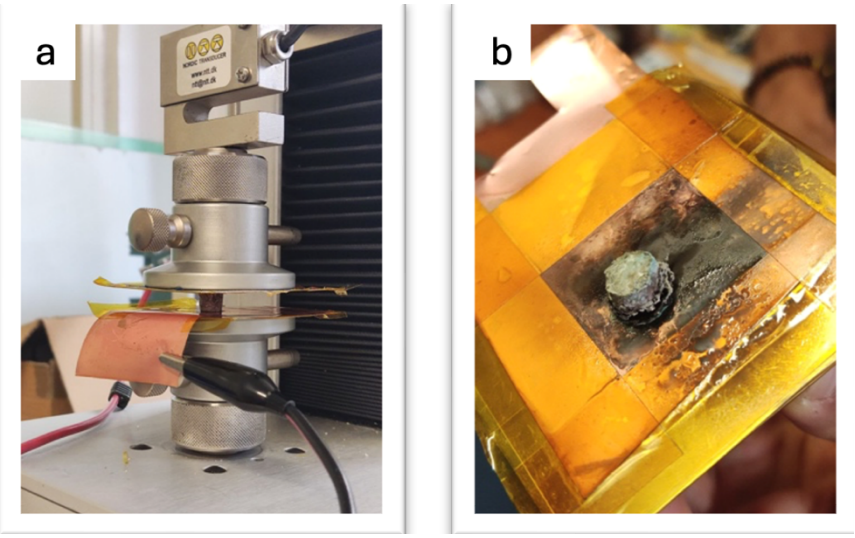

Figure 3-12: a) GelMA/Ag-50 under conductivity test before applying voltage, b) burned sample.

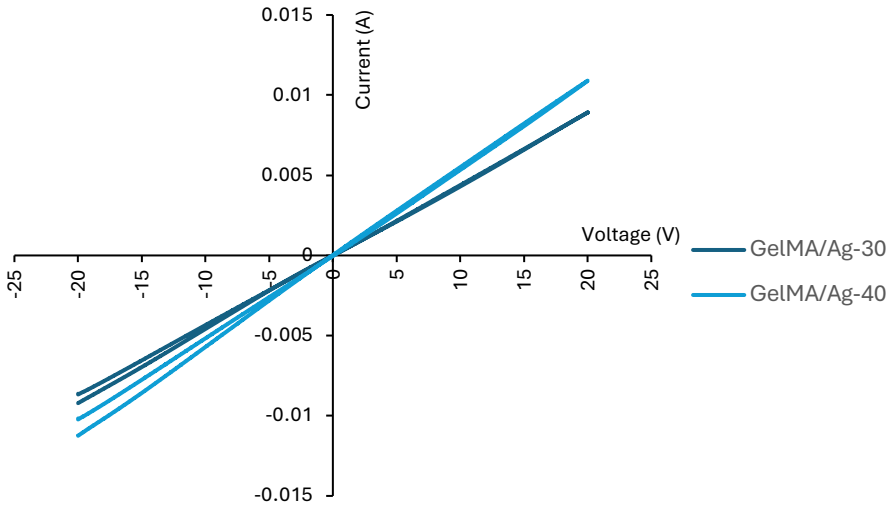

Figure 3-13: Electrical Conductivity of GelMA/silver hydrogels with 72% RH.

Table 3-6: Electrical Characteristics of GelMA/silver hydrogels with 72% RH.

Sample	Quantity of silver inside (g)	Slope (A/V)	Resistance (kΩ)	Resistivity (Ω.m)	Conductivity ($S.m^{-1}$)
GelMA/Ag-30	0.2447	4×10^{-4}	2.5	$1.4\times10^{+1}$	7.09×10^{-2}
GelMA/Ag-40	0.3173	5×10^{-4}	2	$1.18\times10^{+1}$	8.46×10^{-2}
GelMA/Ag-50	0.5368	Burned	Burned	Burned	Burned

For the final phase of testing, the relative humidity was increased to 100% by immersing the samples in distilled water. The applied voltage was reduced to a range of ±1 V to prevent damaging the samples. As expected, the resistance values decreased a lot and reached 24.2 Ω for the GelMA/Ag-50 sample. The GelMA/Ag-30 and GelMA/Ag-40 samples also showed significant conductivity, with resistance values of 222 Ω and 167 Ω, respectively. Complete

hydration significantly enhanced ion mobility within the hydrogel. The current-voltage (I–V) curves have linear and ohmic behavior.

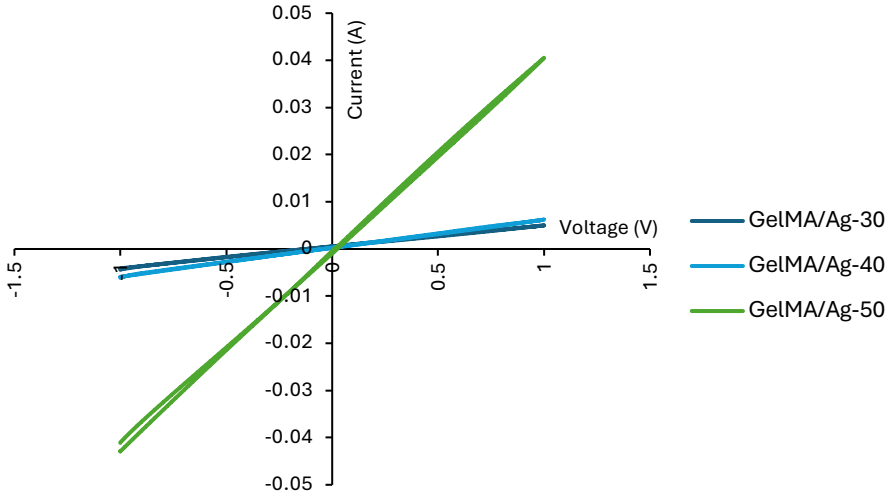

Figure 3-14: Electrical Conductivity of silver-loaded hydrogels with 100% RH.

Table 3-7: Electrical Characteristics of GelMA/Silver hydrogels with 100% RH.

Sample	Quantity of silver inside (g)	Slope (A/V)	Resistance (kΩ)	Resistivity (Ω.m)	Conductivity ($S.m^{-1}$)
GelMA/Ag-30	0.2447	4.5×10^{-3}	2.22×10^{-1}	1.26	0.79
GelMA/Ag-40	0.3173	6×10^{-3}	1.67×10^{-1}	0.99	1.01
GelMA/Ag-50	0.5368	4.12×10^{-2}	2.42×10^{-2}	0.14	6.84

GelMA/ Ag-30 was non-conductive under dry (0% RH) and low-humidity (32% RH) conditions, with resistance values above 200 MΩ. The values displayed on a logarithmic scale highlight the significant difference compared to hydrated states. At 72% RH, the resistance was reduced six orders of magnitude to 2.5 kΩ, and further to 222 Ω in the fully hydrated state, which shows a dramatic increase in conductivity.

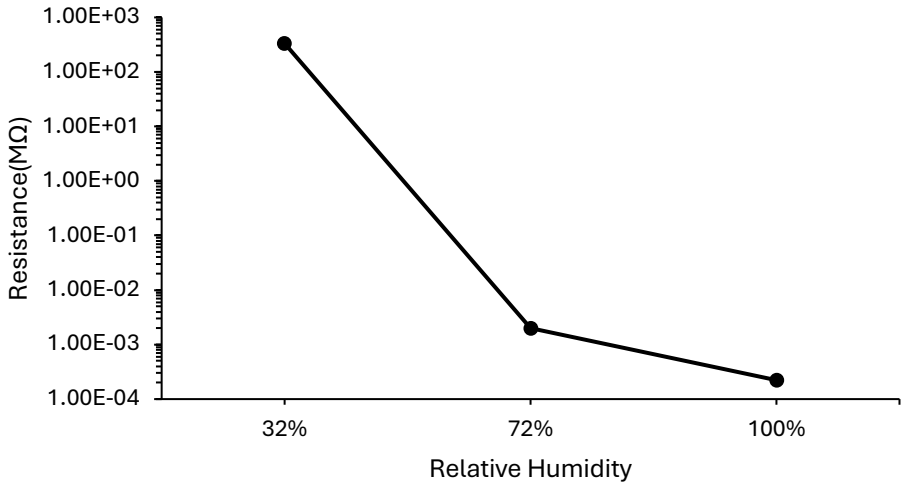

Figure 3-15: Resistance of GelMA/Ag-30 in different humidities.

Like GelMA/Ag-30, GelMA/Ag-40 was non-conductive at low humidity, with resistance values above 500 MΩ at both 0% and 32% RH. As humidity increased to 72% RH, resistance fell to 2 kΩ, and further to 167 Ω under complete hydration. A similar six-order-of-magnitude decrease was also observed in this sample. GelMA/Ag-40, with higher silver content compared to GelMA/Ag-30, also led to an enhancement in conductivity in hydrated states.

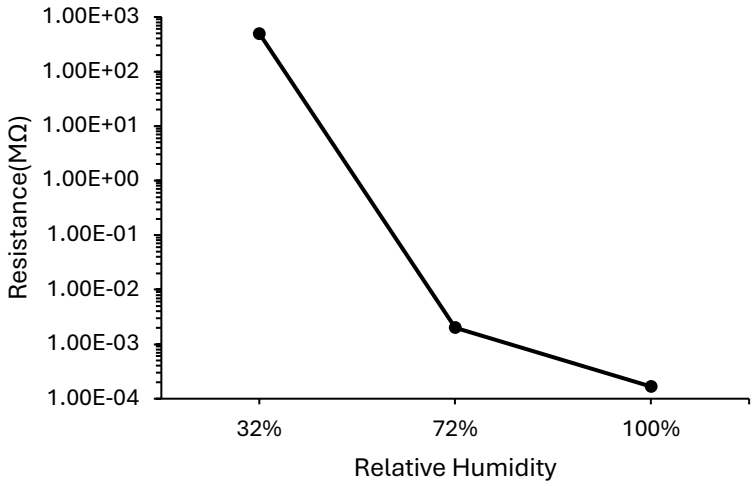

Figure 3-16: Resistance of GelMA/Ag-40 in different humidities.

The GelMA/Ag-50 showed non-conductivity at 0% and 32% relative humidity (RH), similar to two other samples, with resistance values above 500 MΩ. At 72% relative humidity (RH), the sample burned during the experiment. For fully hydrated conditions, the applied voltage was lowered, and the sample showed the highest conductivity among all formulations tested, with a resistance of 24.2 Ω.

The stress-strain curve of hydrated GelMA/Ag hydrogels is shown in Fig. 3-17. This curve indicates elastic deformation in the range of 20 % strain; the slope of each curve illustrates the elastic modulus, which was calculated as 92.48, 108.14, and 119.16 kPa for GelMA/Ag-30, GelMA/Ag-40, and GelMA/Ag-50, respectively. Observations suggest that stiffness is enhanced by increasing the silver content, likely due to the presence of nanoparticles and their reinforcing effect, which enhances the mechanical properties of the hydrogel network. This phenomenon has been observed in a hydrogel system, where incorporation of silver nanoparticles (AgNPs) improved tensile strength and modulus due to strong interfacial interactions between the nanoparticles and the polymer matrix [55].

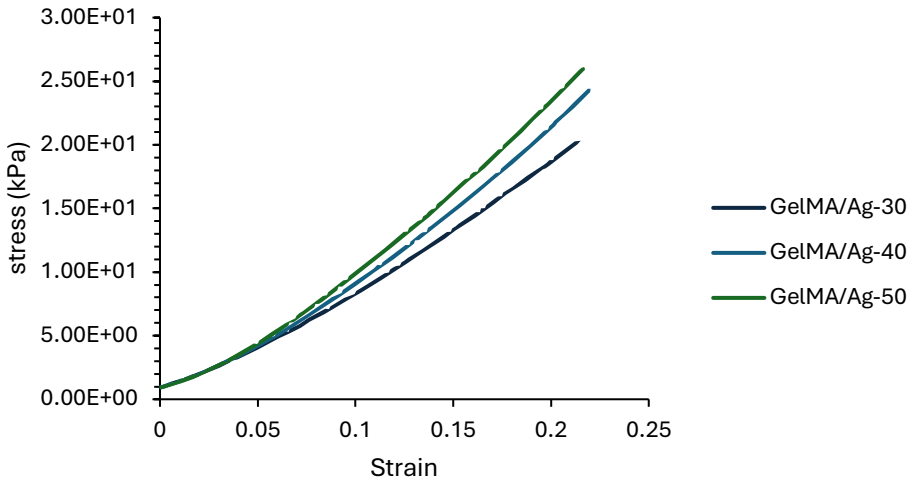

Figure 3-17: stress-strain curve of hydrated GelMA/silver hydrogels.

The piezoresistive behavior of GelMA/silver hydrogels was assessed by observing the change in the current upon applying compressive strain. Electrical current increased with increasing strain, which shows that conductivity is sensitive to applied strain. This observation suggests that applying compression enhances conductivity, likely due to the appearance of a connection between silver nanoparticles, which promote electron transport in addition to an increase in ion mobility within the swollen matrix. In GelMA/Ag-50, the sensitivity of current to applied strain is much more significant in comparison to the other two and indicates that this sample is much more conductive under compression than the other two, which was also observed in the pressure-free test.

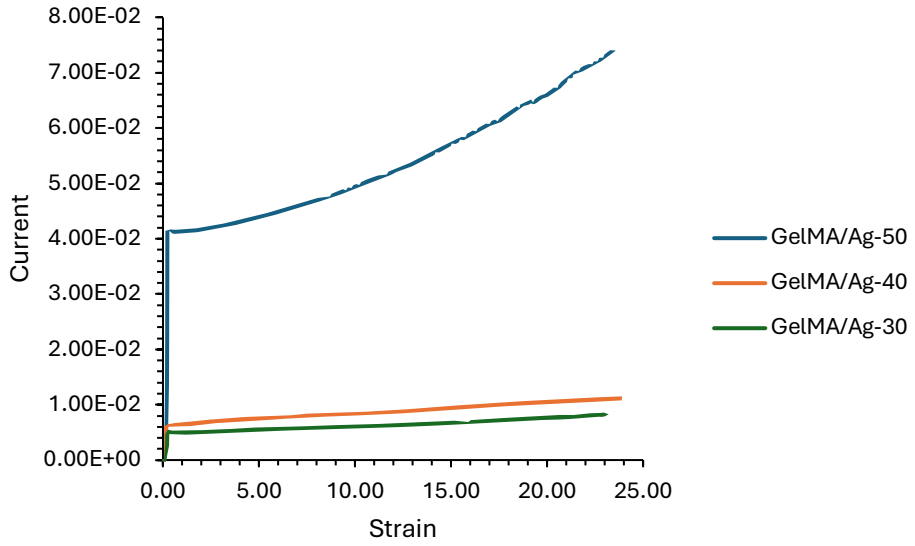

Figure 3-18: Piezoresistive response of hydrated GelMA/silver hydrogels.

In previous research, the conductivity of polyethylene glycol-based hydrogels, unmodified and loaded with silver and gold nanoparticles, was investigated, and it was observed that their conductivity increased by increasing RH from 0% to 100%, and they transitioned from an insulator to a conductive system [56]. Similarly, in my study, a significant drop in resistance occurred as humidity increased in silver-loaded hydrogels, which was attributed to the enhancement of water ions mobility within the swollen hydrogel. A published research [57] reveals that in the hydrated state, water dissociates into ions, such as hydrogen (H^+) and hydroxide (OH^-), and enhances ionic conduction. On the other hand, when the hydrogel swells, the silver nanoparticles may rearrange slightly, reducing gaps and forming conductive pathways. The combination of electron transport and ion mobility lowers the overall resistance. When they were completely dried, the silver nanoparticles could not form a conductive percolation path, and there was no moisture in the network to provide water ion mobility. Therefore, they demonstrated extremely high resistance.

4. Conclusion and outlook

Fish gelatin underwent successful methacrylation and photo-crosslinking and yielded stable hydrogels. The methacrylation process was characterized through Fourier-transform infrared spectroscopy (FTIR). Photorheological analysis demonstrated that the incorporation of approximately 3-4 per hundred resin of BAPO-PEG facilitated rapid curing, with 3 phr identified as optimal to prevent unnecessary material costs associated with excess photoinitiator. The GelMA hydrogels exhibited significant thermal stability, with a decomposition onset temperature (T_{onset}) ranging from approximately 260-270 °C, and demonstrated an ability to absorb around 300% of water, indicative of a hydrophilic porous network. The introduction of silver nitrate ($AgNO_3$), aimed at the incorporation of silver nanoparticles (AgNPs), was achieved through two methodologies: in situ loading and immersion. In both, an obvious color change to brown was observed. In the direct in situ loading method, silver ions Ag^+ influenced photo-crosslinking by preventing light penetration, leading to longer gelation times and slower crosslinking; therefore, the immersion method was preferred.

This study clarifies that the electrical conductivity of GelMA/silver hydrogels is significantly influenced by environmental humidity and the concentration of silver. In the absence of moisture, all tested samples exhibited non-conductive properties, with resistance values in the MΩ range. An increase in relative humidity resulted in a significant decrease in resistance. This decrease occurs due to water dissociation, which enables ion conduction, as well as the slight rearrangement of silver nanoparticles and the formation of a conductive connection path. Complete hydration resulted in the most enhancements in conductivity, particularly in samples with the highest silver content. The piezoresistive properties of GelMA/silver hydrogels were evaluated by observing the change in current in response to applied compressive strain. The results indicated that the current increased by applying strain, which suggests that conductivity is strain-dependent. Applying compression likely improves conductivity by forming connections between silver nanoparticles, causing enhanced electron transport under compression in addition to ion mobility within the swollen matrix. The GelMA/Ag-50 sample exhibited a markedly higher sensitivity compared to the other two samples.

These results highlight the importance of both controlled hydration and optimized silver loading to achieve reliable and effective conductivity in bio-based hydrogels, which is particularly relevant for prospective applications in biosensors, humidity sensors, and soft electronics.

Bibliography

[1] "Hydrogels Based on Natural Polymers," in *Hydrogels Based on Natural Polymers*, Elsevier, 2020, pp. i–iii. doi: 10.1016/b978-0-12-816421-1.00018-5.

[2] "The Method of Small-Angle X-ray Scattering and Its Application to the Structural Analysis of Oligo- and Polysaccharides in Solution," in *Polysaccharide Hydrogels*, Jenny Stanford Publishing, 2015, pp. 281–340. doi: 10.1201/b19751-10.

[3] T. C. Ho *et al.*, "Hydrogels: Properties and Applications in Biomedicine," May 01, 2022, *MDPI*. doi: 10.3390/molecules27092902.

[4] J. M. Dang and K. W. Leong, "Natural polymers for gene delivery and tissue engineering," Jul. 07, 2006. doi: 10.1016/j.addr.2006.03.001.

[5] U. S. K. Madduma-Bandarage and S. V. Madihally, "Synthetic hydrogels: Synthesis, novel trends, and applications," May 15, 2021, *John Wiley and Sons Inc*. doi: 10.1002/app.50376.

[6] J. M. Dodda, K. Deshmukh, D. Bezuidenhout, and Y.-C. Yeh, "Hydrogels: Definition, History, Classifications, Formation, Constitutive Characteristics, and Applications." [Online]. Available: www.rsc.org

[7] E. M. Ahmed, "Hydrogel: Preparation, characterization, and applications: A review," 2015, *Elsevier B.V.* doi: 10.1016/j.jare.2013.07.006.

[8] Y. Lin, H. Zhang, H. Liao, Y. Zhao, and K. Li, "A physically crosslinked, self-healing hydrogel electrolyte for nano-wire PANI flexible supercapacitors," *Chemical Engineering Journal*, vol. 367, pp. 139–148, Jul. 2019, doi: 10.1016/j.cej.2019.02.064.

[9] P. ; Jiménez-Rosado and M. ; Romero, "Novel Trends in Hydrogel Development for Biomedical Applications: A Review," *Polymers (Basel)*, vol. 2022, p. 3023, 2022, doi: 10.3390/polym.

[10] J. Alipal *et al.*, "A review of gelatin: Properties, sources, process, applications, and commercialisation," in *Materials Today: Proceedings*, Elsevier Ltd, 2019, pp. 240–250. doi: 10.1016/j.matpr.2020.12.922.

[11] E. Ali *et al.*, "Gelatin controversies in food, pharmaceuticals, and personal care products: Authentication methods, current status, and future challenges," *Crit Rev Food Sci Nutr*, vol. 58, no. 9, pp. 1495–1511, Jun. 2018, doi: 10.1080/10408398.2016.1264361.

[12] J. M. Joy, A. Padmaprakashan, A. Pradeep, P. T. Paul, R. J. Mannuthy, and S. Mathew, "A Review on Fish Skin-Derived Gelatin: Elucidating the Gelatin Peptides—Preparation, Bioactivity, Mechanistic Insights, and Strategies for Stability Improvement," Sep. 01, 2024, *Multidisciplinary Digital Publishing Institute (MDPI)*. doi: 10.3390/foods13172793.

[13] S. R. Derkach, N. G. Voron'ko, Y. A. Kuchina, and D. S. Kolotova, "Modified fish gelatin as an alternative to mammalian gelatin in modern food technologies," Dec. 01, 2020, *MDPI AG*. doi: 10.3390/polym12123051.

[14] T. Hammer *et al.*, "Mechanically robust non-swelling cold water fish gelatin hydrogels for 3D bioprinting," *Mater Today Bio*, vol. 32, Jun. 2025, doi: 10.1016/j.mtbio.2025.101701.

[15] K. Elkhoury *et al.*, "Synthesis and characterization of C2C12-laden gelatin methacryloyl (GelMA) from marine and mammalian sources," *Int J Biol Macromol*, vol. 183, pp. 918–926, 2021, doi: 10.1016/j.ijbiomac.2021.05.040ï.

[16] J. Venkatesan, S. Anil, S. K. Kim, and M. S. Shim, "Marine fish proteins and peptides for cosmeceuticals: A review," May 01, 2017, *MDPI AG*. doi: 10.3390/md15050143.

[17] A. A. Karim and R. Bhat, “Fish gelatin: properties, challenges, and prospects as an alternative to mammalian gelatins,” 2009, *Elsevier*. doi: 10.1016/j.foodhyd.2008.07.002.
[18] M. B. Aljaber, F. Verisqa, Z. Keskin-Erdogan, K. D. Patel, D. Y. S. Chau, and J. C. Knowles, “Influence of Gelatin Source and Bloom Number on Gelatin Methacryloyl Hydrogels Mechanical and Biological Properties for Muscle Regeneration,” *Biomolecules*, vol. 13, no. 5, May 2023, doi: 10.3390/biom13050811.
[19] S. S. Kordestani *et al.*, “The Effect of Glutaraldehyde on the Properties of Gelatin Films,” 2007. [Online]. Available: https://www.researchgate.net/publication/26488445
[20] N. Tanadchangsaeng *et al.*, “3D bioprinting of fish skin-based gelatin methacryloyl (GelMA) bio-ink for use as a potential skin substitute,” *Sci Rep*, vol. 14, no. 1, p. 23240, Dec. 2024, doi: 10.1038/s41598-024-73774-1.
[21] R. Bhat and A. A. Karim, “Ultraviolet irradiation improves gel strength of fish gelatin,” *Food Chem*, vol. 113, no. 4, pp. 1160–1164, Apr. 2009, doi: 10.1016/j.foodchem.2008.08.039.
[22] A. da T. Alfaro, E. Balbinot, C. I. Weber, I. B. Tonial, and A. Machado-Lunkes, “Fish Gelatin: Characteristics, Functional Properties, Applications and Future Potentials,” Mar. 01, 2015, *Springer Science and Business Media, LLC*. doi: 10.1007/s12393-014-9096-5.
[23] C. Ma *et al.*, “Mammalian and fish gelatin methacryloyl-alginate interpenetrating polymer network hydrogels for tissue engineering,” *ACS Omega*, vol. 6, no. 27, pp. 17433–17441, Jul. 2021, doi: 10.1021/acsomega.1c01806.
[24] H. J. Yoon *et al.*, “Cold water fish gelatin methacryloyl hydrogel for tissue engineering application,” *PLoS One*, vol. 11, no. 10, Oct. 2016, doi: 10.1371/journal.pone.0163902.
[25] N. Celikkin, S. Mastrogiacomo, J. Jaroszewicz, X. F. Walboomers, and W. Swieszkowski, “Gelatin methacrylate scaffold for bone tissue engineering: The influence of polymer concentration,” *J Biomed Mater Res A*, vol. 106, no. 1, pp. 201–209, Jan. 2018, doi: 10.1002/jbm.a.36226.
[26] R. Naomi, H. Bahari, P. M. Ridzuan, and F. Othman, “Natural-based biomaterial for skin wound healing (Gelatin vs. collagen): Expert review,” Jul. 02, 2021, *MDPI AG*. doi: 10.3390/polym13142319.
[27] C. Hermida-Merino *et al.*, “Characterization of Tuna Gelatin-Based Hydrogels as a Matrix for Drug Delivery,” *Gels*, vol. 8, no. 4, Apr. 2022, doi: 10.3390/gels8040237.
[28] K. Liu, S. Wei, L. Song, H. Liu, and T. Wang, “Conductive Hydrogels - A Novel Material: Recent Advances and Future Perspectives,” Jul. 15, 2020, *American Chemical Society*. doi: 10.1021/acs.jafc.0c00642.
[29] S. D. Dutta, K. Ganguly, A. Randhawa, T. V. Patil, D. K. Patel, and K. T. Lim, “Electrically stimulated 3D bioprinting of gelatin-polypyrrole hydrogel with dynamic semi-IPN network induces osteogenesis via collective signaling and immunopolarization,” *Biomaterials*, vol. 294, Mar. 2023, doi: 10.1016/j.biomaterials.2023.121999.
[30] Y. Zhang *et al.*, “Conductive GelMA/PEDOT: PSS Hybrid Hydrogel as a Neural Stem Cell Niche for Treating Cerebral Ischemia-Reperfusion Injury,” *Front Mater*, vol. 9, May 2022, doi: 10.3389/fmats.2022.914994.
[31] X. Qin *et al.*, “Tough, conductive hydrogels based on gelatin and oxidized sodium carboxymethyl cellulose as flexible sensors,” *Carbohydr Polym*, vol. 335, Jul. 2024, doi: 10.1016/j.carbpol.2024.121920.
[32] L. Sun *et al.*, “Induced cardiomyocytes-integrated conductive microneedle patch for treating myocardial infarction,” *Chemical Engineering Journal*, vol. 414, Jun. 2021, doi: 10.1016/j.cej.2021.128723.

[33] A. Navaei, H. Saini, W. Christenson, R. T. Sullivan, R. Ros, and M. Nikkhah, "Gold nanorod-incorporated gelatin-based conductive hydrogels for engineering cardiac tissue constructs," *Acta Biomater*, vol. 41, pp. 133–146, Sep. 2016, doi: 10.1016/j.actbio.2016.05.027.
[34] J. H. Ha *et al.*, "Conductive Gelma–Collagen–Agnw blended hydrogel for smart actuator," *Polymers (Basel)*, vol. 13, no. 8, Apr. 2021, doi: 10.3390/polym13081217.
[35] R. Yan *et al.*, "Skin-interfaced self-powered pressure and strain sensors based on fish gelatin-based hydrogel for wireless wound strain and human motion detection," *Nano Energy*, vol. 118, Dec. 2023, doi: 10.1016/j.nanoen.2023.108932.
[36] F. Ganji, S. Vasheghani-Farahani, and E. Vasheghani-Farahani, "Theoretical Description of Hydrogel Swelling: A Review," 2010. [Online]. Available: www.SID.ir
[37] D. Zhu, L. Jin, Y. Wang, and H. Ren, "Swelling behavior of gelatin-based hydrogel crosslinked with microbial transglutaminase."
[38] J. R. Choi, K. W. Yong, J. Y. Choi, and A. C. Cowie, "Recent advances in photo-crosslinkable hydrogels for biomedical applications," Jan. 01, 2019, *Future Science*. doi: 10.2144/btn-2018-0083.
[39] Y. Yagci, S. Jockusch, and N. J. Turro, "Photoinitiated polymerization: Advances, challenges, and opportunities," Aug. 10, 2010. doi: 10.1021/ma1007545.
[40] J. R. Choi, K. W. Yong, J. Y. Choi, and A. C. Cowie, "Recent advances in photo-crosslinkable hydrogels for biomedical applications," Jan. 01, 2019, *Future Science*. doi: 10.2144/btn-2018-0083.
[41] W. Tomal and J. Ortyl, "Water-soluble photoinitiators in biomedical applications," May 01, 2020, *MDPI AG*. doi: 10.3390/POLYM12051073.
[42] H. Li *et al.*, "PEDOTs-Based Conductive Hydrogels: Design, Fabrications, and Applications," Feb. 19, 2024, *John Wiley and Sons Inc*. doi: 10.1002/adma.202415151.
[43] C. Noè *et al.*, "UV-Cured Chitosan and Gelatin Hydrogels for the Removal of As(V) and Pb(II) from Water," *Polymers (Basel)*, vol. 14, no. 6, Mar. 2022, doi: 10.3390/polym14061268.
[44] R. N. Ghosh *et al.*, "An insight into synthesis, properties and applications of gelatin methacryloyl hydrogel for 3D bioprinting," Oct. 19, 2023, *Royal Society of Chemistry*. doi: 10.1039/d3ma00715d.
[45] W. C. Hou, B. Stuart, R. Howes, and R. G. Zepp, "Sunlight-driven reduction of silver ions by natural organic matter: Formation and transformation of silver nanoparticles," *Environ Sci Technol*, vol. 47, no. 14, pp. 7713–7721, Jul. 2013, doi: 10.1021/es400802w.
[46] A. S. Priya *et al.*, "Comprehensive Review of Hydrogel Synthesis, Characterization, and Emerging Applications," Nov. 01, 2024, *Multidisciplinary Digital Publishing Institute (MDPI)*. doi: 10.3390/jcs8110457.
[47] J. Kong and S. Yu, "Fourier transform infrared spectroscopic analysis of protein secondary structures," *Acta Biochim Biophys Sin (Shanghai)*, vol. 39, no. 8, pp. 549–559, Aug. 2007, doi: 10.1111/j.1745-7270.2007.00320.x.
[48] L. M. Abbas and G. A-R Ahmed, "ATR-FTIR Spectroscopy For Discrimination Of Gelatin From Different Sources: A Comparative Study", doi: 10.33887/rjpbcs/2020.11.4.16.
[49] I. Roppolo *et al.*, "Dual step irradiation process for in situ generation and patterning of silver nanoparticles in a photocured film," *RSC Adv*, vol. 6, no. 18, pp. 14832–14843, 2016, doi: 10.1039/c5ra24234g.
[50] M. F. do Nascimento *et al.*, "UV-polymerizable methacrylated gelatin (GelMA)-based hydrogel containing tannic acids for wound healing," *Drug Deliv Transl Res*, vol. 13, no. 12, pp. 3223–3238, Dec. 2023, doi: 10.1007/s13346-023-01383-y.

[51] C. Qiao and X. Cao, “Swelling Behavior Study of Physically Crosslinked Gelatin Hydrogels,” 2012.
[52] R. Nazar, S. Ronchetti, I. Roppolo, M. Sangermano, and R. M. Bongiovanni, “In situ synthesis of polymer embedded silver nanoparticles via photopolymerization,” *Macromol Mater Eng*, vol. 300, no. 2, pp. 226–233, Feb. 2015, doi: 10.1002/mame.201400204.
[53] A. G. . Ward and A. . Courts, *Humidity Influence to the Thermal and Mechanical Properties of Gelatin Capsules*. Academic Press, 1977.
[54] M. Khan, M. M. Rehman, S. A. Khan, M. Saqib, and W. Y. Kim, “Characterization and performance evaluation of fully biocompatible gelatin-based humidity sensor for health and environmental monitoring,” *Front Mater*, vol. 10, 2023, doi: 10.3389/fmats.2023.1233136.
[55] Y. Liu *et al.*, “Fabrication of gelatin-based printable inks with improved stiffness as well as antibacterial and UV-shielding properties,” *Int J Biol Macromol*, vol. 186, pp. 396–404, Sep. 2021, doi: 10.1016/j.ijbiomac.2021.06.193.
[56] M. Khan, S. Schuster, and M. Zharnikov, “Effect of humidity on electrical conductivity of pristine and nanoparticle-loaded hydrogel nanomembranes,” *Journal of Physical Chemistry C*, vol. 119, no. 25, pp. 14427–14433, Jun. 2015, doi: 10.1021/acs.jpcc.5b03572.
[57] M. Khan, M. M. Rehman, S. A. Khan, M. Saqib, and W. Y. Kim, “Characterization and performance evaluation of fully biocompatible gelatin-based humidity sensor for health and environmental monitoring,” *Front Mater*, vol. 10, 2023, doi: 10.3389/fmats.2023.1233136.

Acknowledgement

I would like to extend my sincere gratitude to my supervisor, Professor Messori, for his support and the opportunity he provided for me to engage in this research endeavor. Additionally, I would like to express my appreciation to my co-supervisor, Dr. Noè, for her invaluable assistance, guidance, and patience throughout this journey. I would also like to convey my honest thanks to Carlo Di Bernardo for his encouragement and insightful guidance.

I want to express my heartfelt gratitude to my parents, Rita and Ali, my wonderful sister and brother-in-law, Mina and Masoud, and the loves of my life, Roshana and Ali. Even though we may be far apart, thinking of them always makes me feel truly overwhelmed with love and appreciation.

I want to extend a warm thank you to my wonderful friends, Saba, Sara, Fardin, and Parham, for standing by me during my challenging times.